UC San Diego
UC San Diego Electronic Theses and Dissertations

## Title
Differences in regulatory motif spacing confer selective responsiveness to type I versus type II interferon signaling.

## Permalink
https://escholarship.org/uc/item/0g45v8g5

## Author
Hodge, Lauren

## Publication Date
2020

Peer reviewed|Thesis/dissertation

eScholarship.org Powered by the California Digital Library
University of California

UNIVERSITY OF CALIFORNIA SAN DIEGO

# Differences in regulatory motif spacing confer selective responsiveness to type I versus type II interferon signaling.

A Thesis submitted in partial satisfaction of the requirements for the degree Master of Science

in

Bioengineering

by

Lauren Hodge

Committee in charge:

Professor Christopher Benner, Chair
Professor Sheng Zhong, Co-chair
Professor Adam Engler
Professor Alon Goren

2020

The Thesis of Lauren Hodge is approved, and it is acceptable in quality and form for publication on microfilm and electronically.

University of California San Diego

2020

# DEDICATION

I dedicate this thesis to my mother, who facilitated my every scientific pursuit starting from my first dissection kit, and to my father and brothers who supported and shared my passions even after enduring years of science fair experiments.

Also, this is to Ashay for being a constant source of both intellectual and emotional support.

EPIGRAPH

“The key to success is to start before you are ready”

-Marie Forleo

“An expert is a person who has made all the mistakes that can be made

in a very narrow field.”

-Niels Bohr

TABLE OF CONTENTS

Signature Page ..... iii

Dedication ..... iv

Epigraph ..... v

Table of Contents ..... vi

List of Figures ..... ix

List of Tables ..... xi

Acknowledgements ..... xii

Abstract of the Thesis ..... xiii

1 Introduction ..... 1

1.1 Innate Immune System ..... 1

1.2 Interferons: Historical and Evolutionary Context ..... 2

1.3.1 Canonical Signaling of Type I Interferons ..... 2

1.3.2 Canonical Signaling of Type II Interferons ..... 4

1.3.3 Type III Interferon ..... 5

1.4.1 Disease Relevance ..... 6

1.4.2 Transcriptional Regulation and Nascent RNA Sequencing ..... 8

1.5 Capped Small RNA Sequencing Defines TSRs at Base Pair Resolution ..... 10

1.6.1 Type-I IFN Signaling Derives Specificity from ISRE Variant ..... 12

2 Results ..... 13

2.1.1 Type I and II IFN Signaling Activate Overlapping Sets of Target Genes in Mouse Macrophages ..... 13

2.1.2 Characterization of Regulatory Element Activation During the IFN Response ..... 15

2.1.3 Measuring Chromatin Accessibility With ATAC-seq ..... 18

2.2 Analysis of DNA Motifs in Interferon Regulatory Elements ..... 21

2.3 T1ISRE is preferentially bound by ISGF3 complex ..... 24

3 Discussion ..... 27

3.1 Summary ..... 27

3.2 Quantifying the Selectivity of the T1ISRE with a Luciferase Reporter Assay ..... 27

3.3 Similar Regulatory Models in Literature ..... 31

3.4 Future Study ..... 31

4 Materials and Methods ..... 33

4.1 Cell culture and treatment ..... 33

4.2 Nuclear RNA Extraction ..... 33

4.3 ATAC-seq ..... 34

4.4 csRNA-seq ..... 34

4.4.1 RNA Precipitation ..... 34

4.4.2 RNA Size Selection ..... 35

4.4.3 5’ Cap Enrichment ..... 35

4.4.4 Library Preparation ..... 36

4.4.5 Bead Size Selection/Gel Purification ..... 37

4.5 Luciferase Reporter Assay Cloning ..... 38

4.5.1 Cloning Native Promoters and Enhancers from RAW264.7 Macrophages ..... 38

4.5.2 Cloning Synthetic Constructs ..... 40

4.5.3 Primer Mutagenesis to Generate Mutated Constructs ..... 40

4.6 NGS Data Analysis ..... 41

4.7 Supplementary Materials ..... 42

4.7.1 Reagents ..... 42

4.7.2 GFP fluorescence in transfected RAW264.7 cells ..... 42

4.7.3 Table of Primers ..... 43

5 References ..... 45

LIST OF FIGURES

**Figure 1: Summary of Canonical IFN Signaling Pathways.** ..... 9

**Figure 2: Overview of csRNA-seq Protocol. A:** Total or nuclear RNA is denatured and run on a 15% Urea-TBE gel for size selection, RNA of length 20-70nt is excised. 10% of RNA is removed for input control..... 11

**Figure 3: Genes induced by IFN-β and IFN-γ have overlapping yet distinct profiles.** Top: tracks are from UCSC Genome Browser showing RNA-seq, csRNA-seq, and ATAC-seq peaks at specified time points. RNA prepped with Illumina TruSeq protocol for total RNA (at the UCSD CORE..... 13

**Figure 4: Experimental Design of IFN Treatment Time-course in RAW264.7 Cells. csRNA-seq:** RAW 264.7 cells were seeded 18 hours before the time-course and treated with either 100U/mL IFN-β, 10ng/mL IFN-γ, or 10ng/mL IFN-λ at time zero..... 15

**Figure 5: Nucleotide Frequency and Read Length Distribution of csRNA-seq Sequencing Reads.** ..... 17

**Figure 6: csRNA-seq defined TSRs at base pair resolution showing temporal response of genes to Type I and Type II IFN. A:** UCSC genome tracks for IRF1, showing csRNA-seq peaks from IFN treatment time course. **B:** UCSC genome tracks for MX2 ..... 17

**Figure 7. RAW264.7 cells do not respond to IFN-L**..... 18

**Figure 8: Changes in ATAC-seq peaks reflect TSR activity in csRNA-seq.** Location of TSR determined by csRNA-seq is denoted by a black arrow ..... 19

**Figure 9: Characterization of Promoter and Enhancer prevalence in TSR peaks**..... 20

**Figure 10: Motif Finding for Interferon Regulatory Elements**. ISRE motif was the highest ranked motif using HOMER ..... 21

**Figure 11: De novo Motif finding.** Left shows top de novo motifs at the 60m treatment timepoint. Right is a heatmap of top enriched motifs, T1ISRE motif outlined by the red box .. 22

**Figure 12: Preferential spacing between GAAA repeats in csRNA-seq and ATAC-seq defined TSRs.** 0: GAAAGAAA, 1: GAAANGAAA (T1ISRE), 2: GAAANNGAAA (ISRE), 3: GAAANNNGAAA, 4: GAAANNNNGAAA..... 23

**Figure 13: Preliminary ChIP data of ISGF3 components overlaps with csRNA-seq peaks enriched for ISRE, T1ISRE, and GAS**..... 24

**Figure 14: Preliminary EMSA data collected by Dr. Chris Benner.** Left: competitive EMSA after stimulating with LPS. Right: stimulation with either LPS, IFN-β, or IFN-γ for 30m and 2 hrs..... 25

**Figure 15: Plasmid map of the TALp-pGRA1-βC+TA reporter plasmid and schematic of the luciferase reporter assay.** See additional details in Materials in Methods ..... 28

LIST OF TABLES

**Table 1: Summary of csRNA Sequencing Results** .....14

**Table 2: Rationalization for Selection of Native Promoter/Enhancer Constructs.** L2FC indicates the normalized log2 fold change in tag counts compared to the nontreatment control. UCSC Browser Coordinates reference the mm10 genome .....28

**Table 3: Mutated Promoter Constructs.** Mutated promoters were generated by primer mutagenesis or E-βlock cloning (see Methods). Bolded sequences are the motif of interest, and the mutations created are in blue .....29

**Table 4**: **Swapped Promoters.** Promoters with swapped motifs. Insertions marked by blue nucleotide, deletions in spacing between GAAA repeats shown underlined.....30

**Table 5: Synthetic Promoters.** Synthetic constructs consist of a random sequence interspersed with five equally spaced motifs of interest, followed by the beta-actin initiation sequence. Synthetic control contains the random sequence without motif insertions, the beta-actin initiation sequence is in bold .....30

**Table 6: NGS Analysis for csRNA-seq Data** ..... 41

**Table 7: Reagent Recipes**.....42

**Table 8: List of Primers** .....44

ACKNOWLEDGEMENTS

I would first like to thank my thesis advisor Dr. Chris Benner for giving me the opportunity to do graduate work in his lab. His continuous encouragement and dedication as a mentor allowed me to gain valuable experimental and bioinformatics skills while becoming an independent researcher, without which this thesis would not have been possible.

I would also like to thank Dr. Alon Goren for his co-mentorship and insightful feedback that have helped me grow as a researcher.

I would like to show sincere gratitude to Dr. Sheng Zhong and Dr. Adam Engler for generously agreeing to be on my thesis committee and for their valuable advice.

Thanks to all the members of the Benner and Heinz lab, especially Dr. Sascha Duttke for his mentorship and phenomenal training on his csRNA-seq method that was the foundation of my thesis work. Special thanks to Dr. Sven Heinz for sharing his expertise in the lab, and whose guidance was instrumental in my research. Thanks also to Carlos Guzman and Camilla Saldanha for their constant advice and support in the lab.

Section 2.1.1 is coauthored with Duttke, Sascha. The thesis author was the primary author of this section.

ABSTRACT OF THE THESIS

Differences in regulatory motif spacing confer selective responsiveness to type I versus type II interferon signaling.

by

Lauren Hodge

Master of Science in Bioengineering

University of California San Diego, 2020

Professor Chris Benner, Chair
Professor Sheng Zhong, Co-chair

The broad role of interferons in innate immune signaling complicates study of their regulatory dynamics. To determine the mechanism underlying the specificity of Type I vs Type II IFN responses, I examined the composition of regulatory elements associated with transcriptional responses specific to each pathway. Here I used csRNA-seq to capture short capped RNAs and identify sites of transcription initiation in both promoters and enhancers at

base-pair resolution. I applied this method to analyze the transcriptional responses in RAW264.7 murine macrophages responding to a time course of stimulation with Type I and Type II Interferon (IFN). I classified differentially regulated promoters and enhancers based on csRNA-seq-enabled identification of these TSRs and supporting ATAC-seq and ChIP-seq data. The time course of stimulation over 4 hours allowed visualization of the temporal dynamics of IFN signaling. I identified a novel variation of the classical Interferon DNA motif, the Interferon Stimulated Response Element (ISRE), called the Type I Interferon Response Element (T1ISRE). The T1ISRE is enriched in the promoters and enhancers of genes preferentially regulated by Type I IFN compared to Type II IFN and is preferentially bound by the ISGF3 complex. This new element underscores how small variations in cis-regulatory sequences can tune transcriptional programs, a strategy observed in other signaling pathways.

# 1 Introduction

## 1.1 Innate Immune System

The ability to distinguish a threat to survival has been a key evolutionary driver in all species, nearly every recorded organism possesses some mechanism of what is defined as innate immunity. It serves as the first line of defense against infectious pathogens and general injury using many of the same effectors that early vertebrates relied on. The innate immune system is designed to respond to general signals of danger rather than recognize a specific pathogen. These “red flags” can be categorized into Danger-associated molecular patterns (DAMPs) and Pathogen-associated molecular patterns (PAMPs). Many PAMPs activate signaling pathways in cells of the innate immune system by binding to their pattern recognition receptors (PRRs) such as TLRs (Takeuchi & Akira, 2010). Phagocytic macrophages are among the first responders to PAMPs, recognizing them either by binding to surface receptors or to intracellular cytoplasmic receptors that bind intracellular ligands of pathogens that have been phagocytosed. Macrophages are derived from monocytes, the myeloid progenitor cells that remain in circulation, differentiating into dendritic cells and macrophages when they invade the surrounding tissue. Macrophages are also involved in the transition between innate and adaptive immunity by presenting antigens derived from phagocytosed material on their surface to lymphocytes, which then results in a specific, adaptive immune response (Wynn et al., 2013).

In addition to phagocytizing pathogens non-specifically or specifically, macrophages are also among the first cells to be activated by patrolling dendritic cells. In order to generate a rapid and strong response, dendritic cells produce immune signaling molecules called cytokines. The class of cytokines known as interferons are primarily produced by dendritic

cells and are a strong activator of macrophages (Diebold et al., 2003). All nucleated cells can respond to Type I IFN; Type II IFN while more specific is critical for a properly orchestrated immune response, making both families key signaling molecules (Stark et al., 1998).

### 1.2 Interferons: Historical and Evolutionary Context

First discovered and functionally characterized by Issacs and Lindenmann in 1957 (*Virus Interference. I. The Interferon*, n.d.)(Lindenmann et al., n.d.), IFNs are a critical link between the innate and adaptive immune responses (Le Bon et al., 2001). They occur earliest in jawless fish, where they evolved from class II helical cytokine ancestor which also gave rise to interleukin-10 cytokine family (Secombes & Zou, 2017). IFNs were named for their interfering effect on viral replication critical for host defense against many viral infections (Carlin et al., 2017) (Ayithan et al., 2015) including influenza (Killip et al., 2015), HCV (Wong & Chen, 2016) and coronaviruses (Kindler et al., 2016). Interferon-stimulated genes (ISGs) activated by interferons are involved in a multitude of pathways including the Mx GTPase pathway, the 2′,5′-oligoadenylate-synthetase-directed ribonuclease L pathway, the protein kinase R pathway and the ISG15 ubiquitin-like pathway (Sadler & Williams, 2008) (Wong & Chen, 2016), though their broader functional roles have been well documented for some time (Stark et al., 1998). Interferons are produced when Toll-like receptors such as TLR3 respond to Pathogen-Associated Molecular Patterns (PAMPs) including dsRNA, the resulting signaling pathway activates the NF-kB and IRF families of TFs which coordinate to bind to the IFN-β promoter to initiate transcription (Takeuchi & Akira, 2010).

#### 1.3.1 Canonical Signaling of Type I Interferons

Type I IFNs are induced by various PAMPs, a common example is dsRNA, a by-product of pathogen replication (Kindler et al., 2016). dsRNA is sensed by toll-like receptor 3

(TLR3) in the endosome, or by RNA helicases RIG-I and MDA5 in the cytoplasm. RIG-I is specific for long dsRNAs and short dsRNAs with a tri- or di-phosphorylated 5' end, while MDA5 senses long dsRNAs with higher-order structure. Downstream signaling pathways activate IRF3, IRF7, and NF-kB, transcription factors that drive expression of genes for IFN-α, IFN-β and other cytokines (Takeuchi & Akira, 2010).

Binding of IFN-α or IFN-β to their receptor IFNAR leads to the activation of two receptor-associated tyrosine kinases, Jak1 and Tyk2; this is followed by tyrosine phosphorylation of the STAT1 and STAT2 proteins. Phosphorylated STAT1 and STAT2 combine with IRF-9 (IFN-regulatory factor 9) to form the trimeric ISGF-3 complex, which, upon translocation to the nucleus, binds to the cis element ISRE (IFN-stimulated response element) 5'-GAAANNGAAA-3', which is present in most IFN-α and IFN-β–responsive genes (Rawlings et al., 2004). Each component of the ISGF3 complex serves a unique function; IRF9 recruits STAT1 and STAT2 to the ISRE, STAT2 contains the transactivation domain, and STAT1 stabilizes the complex and binds the DNA (Qureshi et al., 1995) (Begitt et al., 2014). IFN-β has the highest affinity for both IFNAR receptor halves out of all type I IFNs, and binding affinity is the main source of variation in potency of natural IFNs (Schreiber, 2017), therefore I selected IFN-β as the Type I IFN used for future experiments.

The IFN I pathway is heavily centered on antiviral activity, and often the response is rapid but transient as some gene products are toxic to the cells after long periods of exposure. The dynamics and timing of IFN-I signaling can be crucial especially in the case of viral infection; a delayed IFN-I response in SARS-CoV-2 infected mice can exacerbate an overactive inflammatory response leading to the associated vascular leakage, tissue damage, and increased mortality (Channappanavar et al., 2016). This follows similar disease patterns

previously observed in patients with severe SARS (Franks et al., 2003).

### 1.3.2 Canonical Signaling of Type II Interferons

IFN-γ is the only member of the Type II IFN family and at the time of its discovery was thought to be nearly indistinguishable from Type I IFN, though it has unique functions including regulation of T cells, B cells, and granulocytes. Of the IFNs, IFN-γ is the most effective inducer of MHC class II antigens in macrophages via its upregulation of CIITA (MHC class II master regulator) for antigen-presenting cells (Steimle et al., 1994). IFN-γ also has important roles in pathogen defense against mycobacteria; in patients with genetic or acquired defects/deficiencies of IFN-γ or its receptor subunits, increased susceptibility, disease severity, and poor outcomes have been observed (Murray, 1994).

The classification of IFN-β as antiviral and IFN-γ as broadly immunomodulatory is an oversimplification, as IFN-γ is critical for a proper antiviral response against HCV due to its direct inhibition of replication in addition to enhancing natural killer cell activity and antigen presentation of dendritic cells to T cells (Thimme et al., 2001). IFN-γ is also proinflammatory and plays an important role in the development of nephritis in preclinical lupus models and Guillain-Barre syndrome (Hu & Ivashkiv, 2009) (Pollard et al., 2013). In contrast to type I IFN, binding of IFN-γ to its receptor leads to tyrosine phosphorylation of the Jak1 and Jak2 tyrosine kinases, resulting in the phosphorylation of STAT1 but not STAT2. Phosphorylated STAT1 homodimerizes to form the Gamma Activating Factor (GAF) which translocates to the nucleus and binds to the IFN-γ activation site (GAS) element present in most IFN-γ–inducible genes. IFN-γ can also activate STAT1-independent pathways, either dependent or independent of Jak1 and Jak2 (Ramana et al., 2002), and the downstream pathways often stimulate other STAT family members in a cell-type specific manner (van Boxel-Dezaire &

Stark, 2007).

### 1.3.3 Type III Interferon

The Type III IFN family was discovered in 2003 (Kotenko et al., 2003) (Sheppard et al., 2003) and consists of IFN-λ1-4. They signal through a receptor complex composed of IFN-λR1-unique to IFN-λ- and IL-10R2 which is shared with the receptor complexes for IL-10. IL-22, and IL-26, and the downstream signaling pathway activated largely overlaps with that of Type I IFNs. IFN-λ binds to the IFN-λR1 chain which quickly undergoes a confirmation change to recruit the complementary IL-10R2 chain. The fully formed complex recruits Jak1 and Tyk2, which catalyze transphosphorylation of the receptor chains allowing for recruitment of STAT1 and STAT2. STAT1 and STAT2 are phosphorylated, and IRF9 is recruited to form the ISGF3 complex (Donnelly & Kotenko, 2010).

Given that the downstream signaling pathway of IFN- λ largely overlaps with that of Type I IFNs, it's non-redundant role stems from the tissue specificity of its receptor. IFN-λR1 is primarily expressed in epithelial cells (Hemann et al., 2017) explaining the protective role of IFN-λ in antiviral defenses against respiratory pathogens such as pulmonary influenza (Jewell et al., 2010) and SARS-CoV-2 (Jafarzadeh et al., 2020) as well as other viral infections in the gut where IFN-III but not IFN-I was critical for preventing viral replication (Pott et al., 2011). Response of immune cells to IFN-λ differs widely by cell type; myeloid lineages such as dendritic cells and neutrophils, while NK cells and T cells have minimal responses. Macrophages are sensitive to IFN-λ, however monocytes have minimal expression of IFN-λR1 and therefore do not respond to IFN-λ (Read et al., 2019). It has been previously shown that RAW264.7 cells which are monocyte/macrophage-like do not respond to IFN-λ (Pott et al., 2011). I decided to verify this by including IFN-λ as one of my treatment conditions for

RAW264.7 cells.

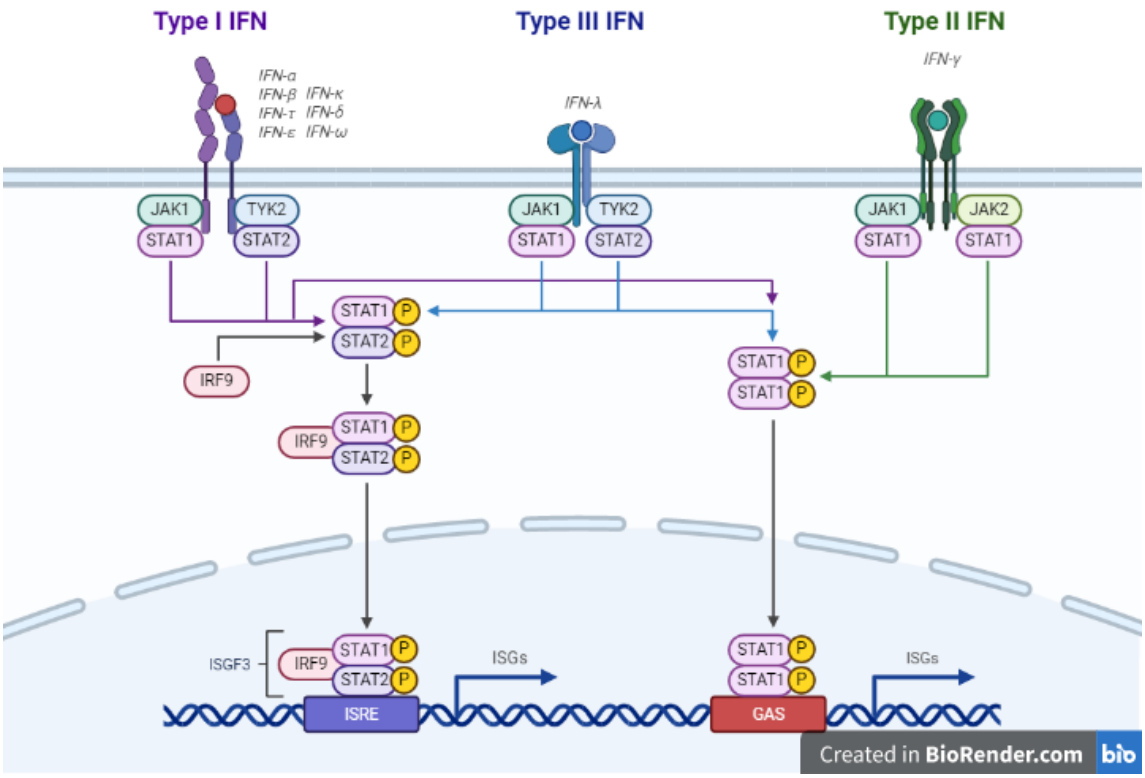


**Figure 1: Summary of Canonical Interferon Signaling Pathways.**

### 1.4.1 Disease Relevance

The complicated involvement of interferons in both protective and disease-associated inflammatory pathways is evident in historical reviews of clinical trials using interferons as candidate treatments for various diseases (Antonelli et al., 2015). Dysregulation of IFN-α is a common factor in multiple autoimmune rheumatic diseases such as Systemic lupus erythematosus, Type 1 diabetes, and multiple sclerosis (Niewold, 2014) however trials targeting IFN-I often fail because they only work for certain subpopulations (Psarras et al., 2017). Type I IFN has also been considered a candidate for cancer immunotherapy due to its effective recruiting of effector T cells to tumors and dendritic cell activation, though its success in trails is mixed (Hervas-Stubbs et al., 2011).

IFN-γ has a similarly complicated involvement in atherosclerosis. Its roles in disease progression include inducing dysregulation of cholesterol homeostasis leading to foam cell formation; increasing release of chemokines which recruit monocytes and CD4+ T-lymphocytes to the atherosclerotic lesion, and inducing expression of adhesion molecules that increase infiltration of monocytes to the region (McLaren & Ramji, 2009). However, IFN-γ can also be atheroprotective, inhibiting the oxidation of LDL and decreasing LDL expression in macrophages by increasing the expression of the antioxidant inducible nitric oxide synthase (iNOS) (McLaren & Ramji, 2009).

Many antimicrobials used by innate immune system, particularly those activated by Type I Interferon are self-toxic; therefore, the temporal control of downstream signaling is of utmost importance. Dysregulation of the dynamics and timing of IFN-I signaling correlates strongly with poor disease outcomes, particularly with respect to viral infections. The recently discovered SARS-CoV-2 exploits this by delaying IFN-I responses at multiple points in the signaling pathway; viral protein ORF6 blocks translocation of STAT1 and other transcription factors into the nucleus preventing downstream signaling, while Nsp6 binds TBK1 to prevents phosphorylation and subsequent activation of interferon regulatory factor 3 (IRF3) (Xia et al., 2020). The delayed antiviral response of Type I IFN appears to be crucial for successful viral replication, as the number of viral transcripts increases significantly before IFN-I induction in SARS-CoV-2 infected cells, and treatment of IFN-β blocks SARS-CoV-2 replication. This critical “window of opportunity” created by the delayed Type I IFN response also appears to be associated with an overzealous immune response in COVID-19 patients characterized by excessive production of pro-inflammatory cytokines such as IL-6, TNF, and others (Lei et al., 2020). The conflicting evidence of both positive and negative

effects of IFN-I in clinical trials appears to be at least partially explained by the timing of treatment; early-on in the infection course IFN-I appears to have a protective role while treatments at a later stage can exacerbate inflammation, leading to increased mortality and delayed recovery (Wang et al., 2020).

Many of these disparate effects likely arise because Type I and Type II IFNs are broadly proinflammatory cytokines with involvement in diverse immune pathways that exhibit significant crosstalk, the pathways activate common and specific target genes. Interestingly, separate gene targets of both pathways are highly enriched for ISREs in their promoters, suggesting there is another mechanism responsible for IFN-I specific activity. Determining the source of specificity requires an understanding of the regulatory components involved.

### 1.4.2 Transcriptional Regulation and Nascent RNA Sequencing

Transcription initiation begins when RNAPII is recruited by the pre-initiation complex (PIC) consisting of six general transcription factors (TFIIA, TFIIB, TFIID, TFIIE, TFIIF, TFIIH) to bind to a sequence immediately upstream of the gene called the promoter. Transcriptional start sites (TSSs) are defined where the RNAPII begins transcribing RNA. The core promoter is the region between -50 and +50 of the initial RNAPII binding site; and can contain various canonical sequences such as the TATA box, TFIID subunit binding site, initiation sequence, TFIIB recognition element (BRE), and downstream promoter elements (DPEs). Most mammalian promoters contain an initiation sequence; however, the other components are not always necessary or present. The classical understanding of transcription often relies on a focused promoter model for transcription initiation, where transcription initiates from one specific site. However, mammalian genes often have dispersed promoters

where transcription initiation occurs in multiple sites in a certain region of the promoter (Juven-Gershon et al., 2008). Therefore, it is more accurate to refer to the region of the promoter where transcription initiates as the Transcriptional Start Region (TSR).

Regulation of transcription occurs at multiple levels to obtain spatial and temporal control. These regulatory levels can be described in order of their role in transcription as they occur, from assembly of the pre-initiation complex to recruitment of RNAPII, additional transcription factor binding, initiation of transcription, and RNAPII pausing, as well as adjacent processes including chromatin structure influenced by nucleosome positioning and histone modifications. The discussion of transcriptional regulation in this thesis will primarily focus on the initiation of transcription, the impact of DNA motifs in their recruitment of transcription factors, and the cis-regulatory elements involved.

Cis-regulatory elements are non-coding DNA sequences are involved in regulation of gene expression, they include proximal promoters, enhancers, silencers, and boundary elements (Wittkopp & Kalay, 2012). As discussed previously, the region upstream of a gene that initiates and controls transcription usually includes more elements in addition to a core promoter, but these elements can vary considerably. Determining the specific sequence within a given region upstream of a gene with the most influence on transcription relies largely on functional experimental validation for each section of the promoter, a difficult task to scale up. For practical purposes, proximal promoters are therefore generally defined as encompassing the region around the core promoter from -250 to +250 bp, including the RNAPII binding site, though the region size can vary (Wittkopp & Kalay, 2012). In contrast, enhancers are often located in noncoding and intronic regions hundreds of kilobases away from the TSS of a gene regulated by them. Enhancers are defined by their ability to regulate transcription independent

of their orientation or distance to a target gene and a single enhancer can regulate multiple distant genes (Andersson et al., 2014). This functional definition is useful, but it makes discovery and classification of enhancers a challenge. Often histone modifications such as H3K27ac or the ratio of H3K4me1 to H3K4me3 are used as a marker for enhancers since their signature is thought to be unique compared to promoter regions (Heintzman et al. 2007). However, these histone markers have comparatively low resolution, only able to define general regions of chromatin. In order to pinpoint more unique sequence features a new class of sequencing methods was developed aimed at isolating newly transcribed, or nascent RNAs (Wissink et al., 2019). These include run-on sequencing reactions like GRO-seq (Core et al., 2008), PRO-seq which map active Pol II positions at nucleotide resolution genome-wide (Kwak et al., 2013), and 5' GRO-seq isolates 5' capped RNAs (Lam et al., 2013). There are also methods that focus on RNAs currently associated with RNAPII such as NETseq (Churchman & Weissman, 2011). TT-seq, or transient transcriptome sequencing, maps stable and transient RNAs and estimates rates of synthesis and degradation (Schwalb et al., 2016). These methods have revolutionized RNA sequencing but they have certain caveats, GRO-seq and 5' GRO-seq use labeled NTPs, PRO-seq requires biotin-affinity purification, RNAPII is epitope-tagged for NET-seq, and TT-seq uses metabolic labeling; therefore all above methods are limited to artificial cell culture applications.

### 1.5 Capped Small RNA Sequencing Defines TSRs at Base Pair Resolution

csRNA-seq was developed as a way to assay nascent RNAs at single base-pair resolution that can be applied to total RNA allowing analysis of samples from frozen tissue or other in vivo applications (Duttke et al., 2019). This is done by first isolating and size selecting RNAs between 20-70 nucleotides on a denaturing urea gel. These short RNAs will

contain noncapped RNAs (ribosomal rRNA and miRNAs) and other undesirable species like capped miRNA precursors. The sample is then treated with a 5'-phosphate dependent exonuclease, which selectively degrades 5' monophosphorylated RNAs like rRNAs, but does not affect capped or di/tri-phosphorylated RNAs. Next the triphosphorylated miRNAs are depleted by treatment with alkaline phosphatase, leaving the sample enriched for RNAs with a 5' 7-methylguanosine cap. Before these 5' cap enrichment steps, 10% of the RNA is set aside to be used as an input control; this RNA will contain more degraded RNAs as well as miRNAs, rRNAs, etc. This input RNA is useful when defining TSRs as a peak from the csRNA-seq sample that matches an input peak in location and intensity is likely a false TSR. After the cap enrichment the input samples are added back into the protocol, and all RNA is de-capped by 5' pyrophosphorylase before the library preparation. First the 3' adaptor is ligated, then the RT primer is annealed to the 3' adaptor to minimize formation of adaptor dimers. Next the 5' adaptor is ligated, then the samples undergo reverse transcription and PCR barcoding. A second round of size selection is done, first with magnetic beads then by gel size selection to further minimize the presence of adapter dimers and concatemers, then the samples are purified, pooled, and sequenced.

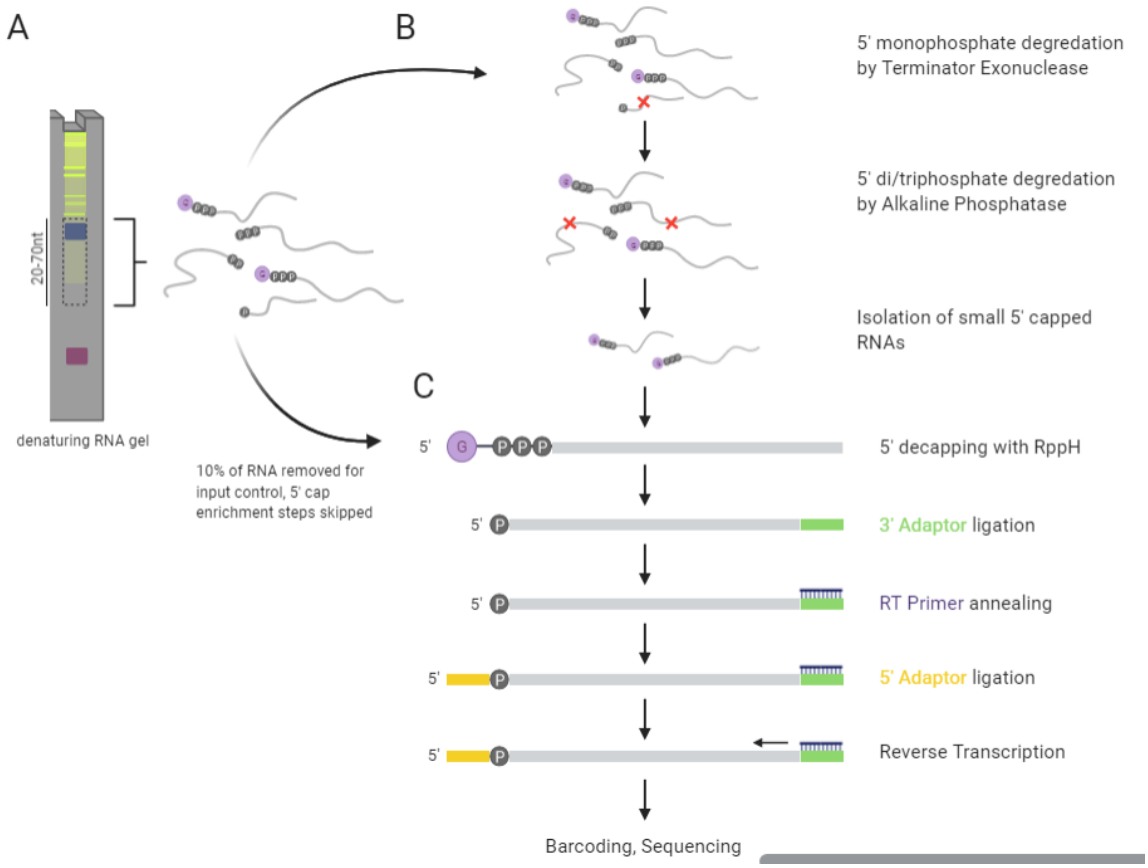


**Figure 2: Overview of csRNA-seq. A:** Total or nuclear RNA is denatured and run on a 15% Urea-TBE gel for size selection, RNA of length 20-70nt is excised. 10% of RNA is removed for input control. **B:** 5' cap enrichment done to select for RNAs with a 5'7-methylguanosine cap and deplete rRNAs, miRNAs, etc. **C:** Library preparation, RNA de-capped, adaptors added sequentially, then samples reverse transcribed and PCR barcoded for sequencing.

### 1.6.1 Type-I IFN Signaling Derives Specificity from ISRE Variant

These advances in sequencing methods have allowed us to capture subtleties of transcriptional regulation previously unknown by identification of cis-regulatory elements that give insight into how Type I IFN elicits a unique transcriptional response. Using the macrophage-like mouse cell line RAW 264.7, I employed the novel sequencing method csRNA-seq in conjunction with other well-established methods assaying chromatin accessibility, gene expression, and chromatin markers. With the data taken together, we identified a novel regulatory element hereafter named the Type I Interferon Response Element (T1ISRE), a novel version of the traditional ISRE that is more specific to Type I IFN

signaling. We propose that the T1ISRE is specifically bound and activated by the ISGF3 complex, while traditional ISREs are also capable of binding IRF dimers.

# 2 Results

### 2.1.1 Type I and II IFN Signaling Activate Overlapping Sets of Target Genes in Mouse Macrophages

To investigate similarities and differences in IFN signaling, we treated RAW264.7 murine macrophage cells with IFN-β or IFN-y extracted RNA from 1h and 4h post-treatment and performed RNA-seq prepped with Illumina TruSeq protocol for total RNA.

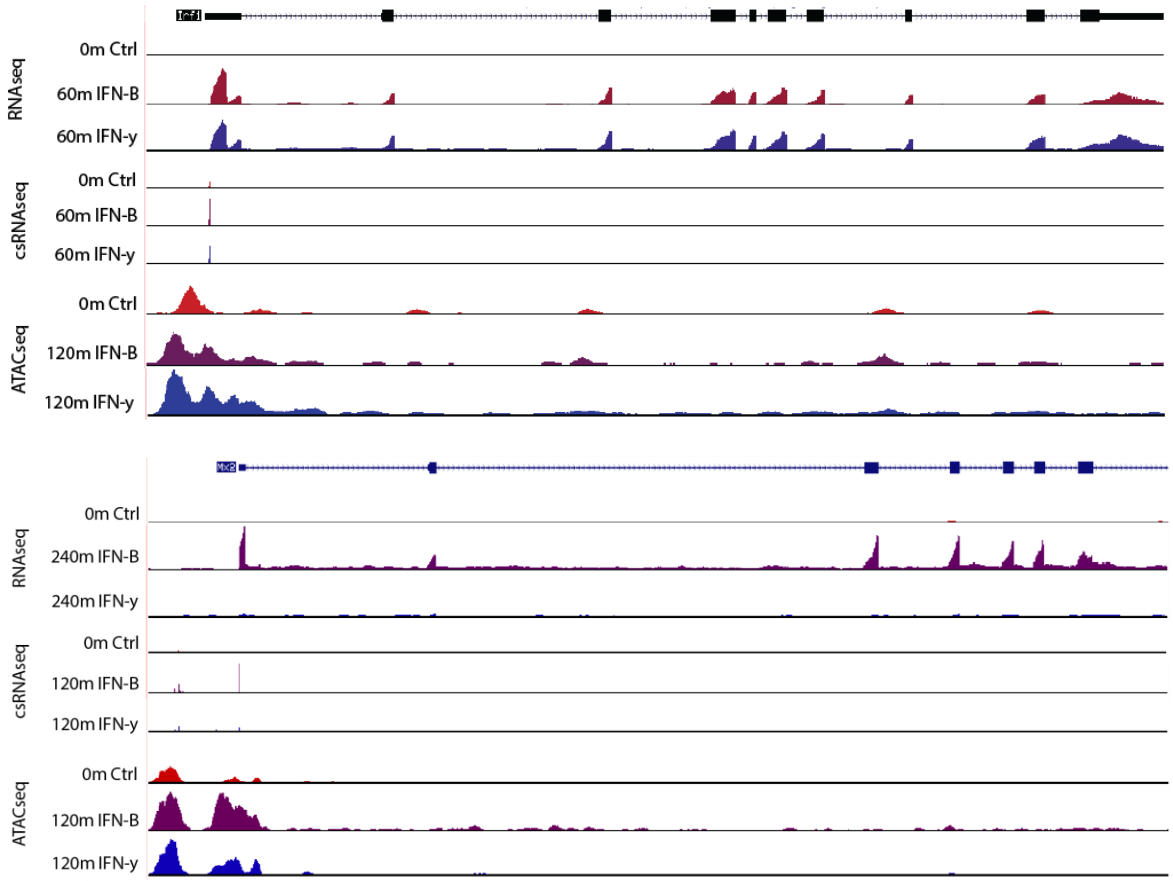


**Figure 3: Genes induced by IFN-β and IFN-γ have overlapping yet distinct profiles.** Top: tracks are from UCSC Genome Browser showing RNA-seq, csRNA-seq, and ATAC-seq peaks at specified time points. RNA prepped with Illumina TruSeq protocol for total RNA (at the UCSD CORE). Bottom: bar graphs are Metascape analysis results at the 60m timepoint showing top biological processes upregulated by either IFN-β or IFN-γ.

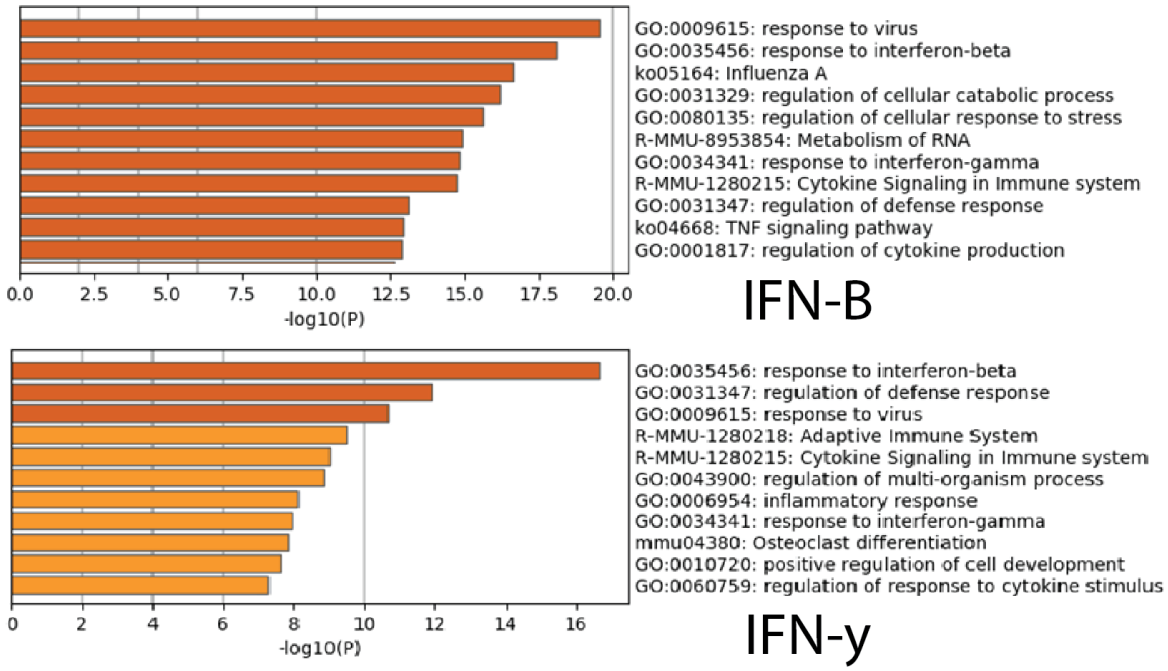


**Figure 3: Genes induced by IFN-β and IFN-γ have overlapping yet distinct profiles continued.** Top: tracks are from UCSC Genome Browser showing RNA-seq, csRNA-seq, and ATAC-seq peaks at specified time points. RNA prepped with Illumina TruSeq protocol for total RNA (at the UCSD CORE). Bottom: bar graphs are Metascape analysis results at the 60m timepoint showing top biological processes upregulated by either IFN-β or IFN-γ.

Interferon Regulatory Factor IRF1 is known to be induced by Type I and Type I IFN, the top panel in Figure 3 shows the increase in mRNA expression from RNA-seq data, the pronounced TSRs identified with csRNA-seq, and the change in chromatin accessibility visualized from ATAC-seq data. Mx2 is a strong antiviral effector preferentially induced by IFN-β over IFN-y (Der et al., 1998), all sequencing data obtained shown in Figure 3 reflects this behavior. Metascape analysis was based on the top 2500 genes with the greatest log2 fold change in IFN-β or IFN-γ treatment at the 60-minute time point compared to the non-treatment control (Zhou et al., 2019). Resulting enriched biological processes showed overlap of pathways upregulated by IFN-β and IFN-γ. Overall, I confirmed that the genes induced by IFN-β and IFN-γ treatment are involved in innate immune signaling pathways, and data agrees with previous literature on which targets are common or specific to Type I IFN.

Section 2.1.1 is coauthored with Duttke, Sascha. The thesis author was the primary author of this section.

### 2.1.2 Characterization of Regulatory Element Activation During the IFN Response

I decided to leverage the single-nucleotide resolution allowed by csRNA-seq to interrogate the unique responses of RAW264.7 macrophages to Type I and Type II Interferon and capture the temporal dynamics by doing a time-course of treatment, shown in Figure 4. Profiling shows marked changes in transcription both at promoters and pre-defined enhancers.

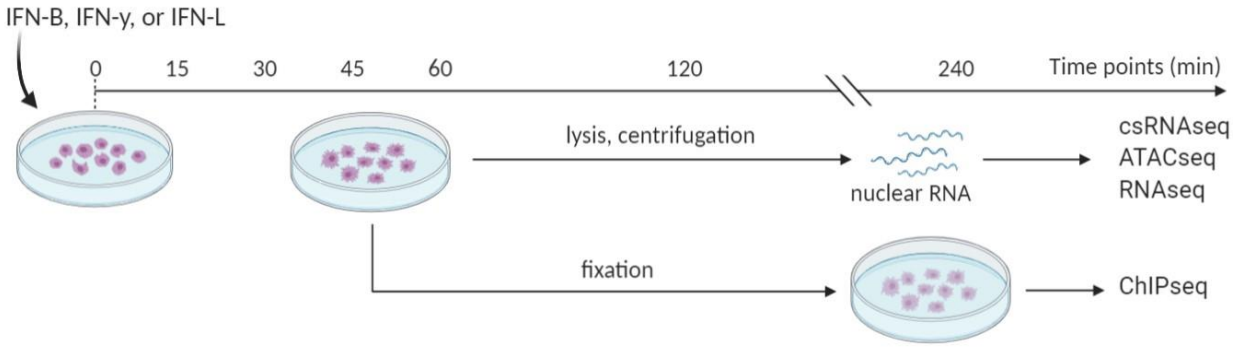


**Figure 4: Experimental Design of IFN Treatment Time course in Macrophage Cells. csRNA-seq:** RAW 264.7 cells were seeded 18 hours before the time course and treated with either 100U/mL IFN-β, 10ng/mL IFN-γ, or 10ng/mL IFN-L at time zero. **csRNA-seq/ATAC-seq:** Nuclei from were isolated and counted, 250k were used for ATAC-seq, remainder were used for csRNA-seq. **ChIP-seq:** Cells were double-crosslinked with 2mM DSG and 1% Formaldehyde and proceeded with ChIP-seq for STAT1, STAT2, IRF9. **RNA-seq:** Cells from the 0, 60m, and 240m time point were harvested. For details of these methods refer to the Material and Methods section.

At each time point libraries were prepared and sequenced at depths described in Table 1 and aligned to the mm10 mouse genome assembly using STAR. This initial round of sequencing in Table 1 had lower % alignment for the csRNA-seq samples. A significant percentage of reads corresponded to adaptor dimers due to improper size selection during the second gel (10% TBE) after barcoding. During subsequent rounds of csRNA-seq the gel was cut at least 1mm above the top of the adaptor dimer band to minimize their contamination of the samples (example gel photos in Supplemental Materials).

**Table 1: Summary of csRNA Sequencing Results.**

| Sample Name | Total reads | % Adapter Dimers | % Aligned |
|---|---|---|---|
| RAW-csRNA-ctrl-000m-LH031-200316 | 13816959 | 29.90% | 65.80% |
| RAW-csRNA-ctrl-360m-LH033-200316 | 8809923 | 45.70% | 44.40% |
| RAW-csRNA-IFNb-015m-LH007-200316 | 14039248 | 28.90% | 64.70% |
| RAW-csRNA-IFNb-030m-LH009-200316 | 8996052 | 46.90% | 44.10% |
| RAW-csRNA-IFNb-045m-LH011-200316 | 12778606 | 32.50% | 59.70% |
| RAW-csRNA-IFNb-060m-LH013-200316 | 9151401 | 23.70% | 70.40% |
| RAW-csRNA-IFNb-120m-LH015-200316 | 12113666 | 28.70% | 64.30% |
| RAW-csRNA-IFNb-360m-LH017-200316 | 1977422 | 45.60% | 44.80% |
| RAW-csRNA-IFNg-015m-LH019-200316 | 11764774 | 31.40% | 58.60% |
| RAW-csRNA-IFNg-030m-LH021-200316 | 9320308 | 19.30% | 75.50% |
| RAW-csRNA-IFNg-045m-LH023-200316 | 7212315 | 21.20% | 72.50% |
| RAW-csRNA-IFNg-060m-LH025-200316 | 4543339 | 37.80% | 54.40% |
| RAW-csRNA-IFNg-120m-LH027-200316 | 9107124 | 21.40% | 72.20% |
| RAW-csRNA-IFNg-360m-LH029-200316 | 4216208 | 36.70% | 51.90% |

The csRNA-seq samples were compared with their corresponding non-5'cap-enriched inputs to filter out high abundance RNAs that would bias TSR discovery. The majority of input RNAs are sourced from introns, intergenic regions containing snoRNAs and miRNAs, promoters, and 3' and 5' UTR regions. I analyzed the architecture of the TSRs identified by csRNA-seq as a proof of concept for the method. I first found the peaks in each sample relative to its input to correct for highly prevalent miRNAs, snoRNAs, etc, then I created a histogram of the nucleotide frequencies relative to the transcription initiation position, shown in Figure 5. There is a clear initiator CA dinucleotide present in both the input and csRNA-seq samples, but in the cap-enriched csRNA-seq sample it is far more pronounced. The samples also show a spike around -30bp indicating the presence of a TATA box not visible in the input. Finally, about 50bp after initiation a regular pattern emerges in the csRNA-seq samples showing nucleotide frequency variation due to nucleosome positioning. Next I generated a histogram of read length for the samples and inputs, shown in the bottom panel of Figure 5. The inputs showed a strong peak at 22bp corresponding to miRNAs, while the csRNA-seq samples had a broader distribution

indicating less bias for one particular RNA species.

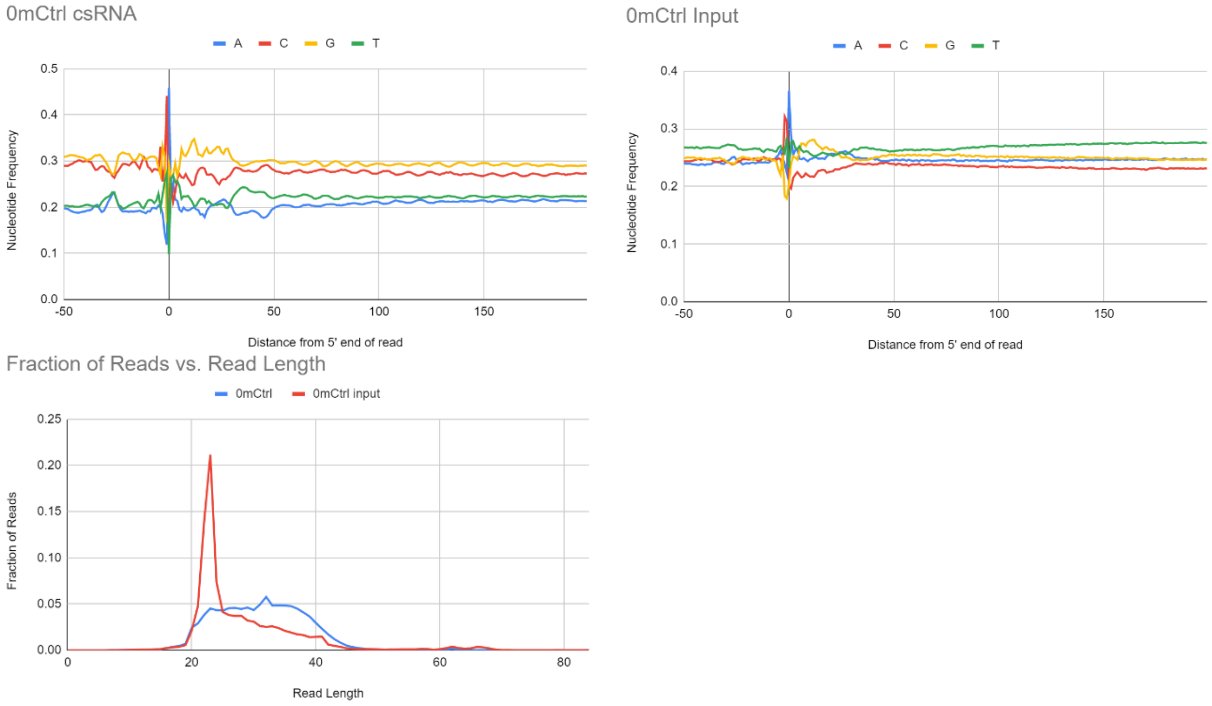


**Figure 5: Nucleotide Frequency and Read Length Distribution of csRNA-seq Sequencing Reads.** Top: bar graphs measure nucleotide frequency in the genome, measuring the distance to the 5' end of the csRNA-seq reads. Bottom: read length distribution of csRNA-seq vs input reads.

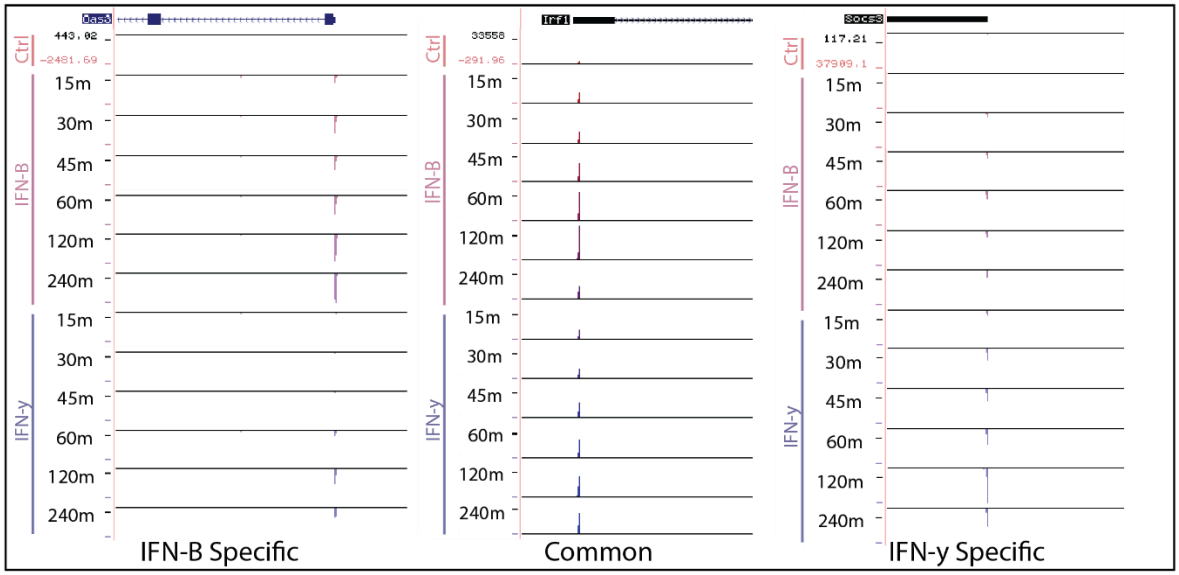


**Figure 6: csRNA-seq defined TSRs at base pair resolution showing temporal response of genes to Type I and Type II IFN.** A: UCSC genome tracks for IRF1, showing csRNA-seq peaks from IFN treatment time course. B: UCSC genome tracks for MX2.

The time-course data allowed me to show that while certain genes are induced by both IFN-β and IFN-γ, there are differences in the timing; in Figure 6 Oas3 was significantly upregulated by both IFN-β and IFN-γ but the response to IFN-β is much more rapid.

I also confirmed that IFN-L does not elicit a response in RAW264.7 macrophages, shown in Figure 7. IRF-1 is a classical target of ISGF3, the transcription factor complex induced by both IFN-I and IFN-III (and IFN-II to a lesser extent).

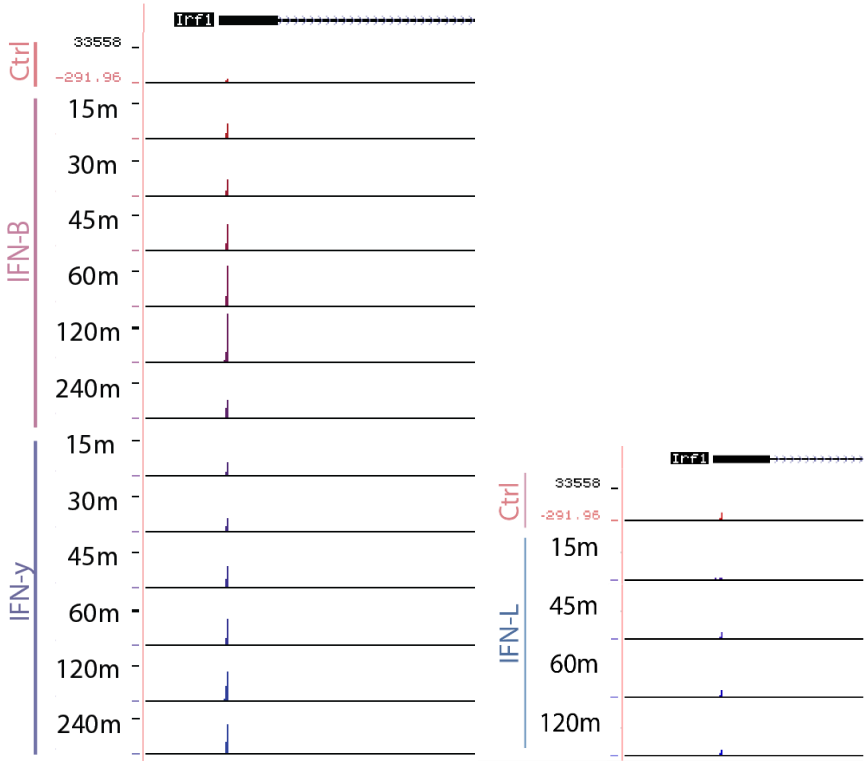


**Figure 7: RAW264.7 cells do not respond to IFN-L.** IFN-L treatment timepoints with comparatively low sequencing depth were removed.

### 2.1.3 Measuring Chromatin Accessibility With ATAC-seq

ATAC-seq is an NGS method that sequences open chromatin as a way of quantifying chromatin accessibility and therefore indirectly estimates transcriptional activity (Buenrostro et al., 2013). It is particularly useful when investigating unknown regulatory elements since it surveys open chromatin in an unbiased manner. It employs the active transposase Tn5 with NGS

adapters; the Tn5 will integrate these adapters into regions of open chromatin, while regions of closed chromatin will remain too tightly packed to allow for transposase activity. After harvesting RAW264.7 macrophages from the IFN-β and IFN-γ treatment time-course and isolating nuclei, I aliquoted 250k nuclei per sample for ATAC-seq to be done in parallel with csRNA-seq. This allowed comparison of direct measurements of changes in transcription with changes in the open chromatin, aiding in discovery of regulatory elements.

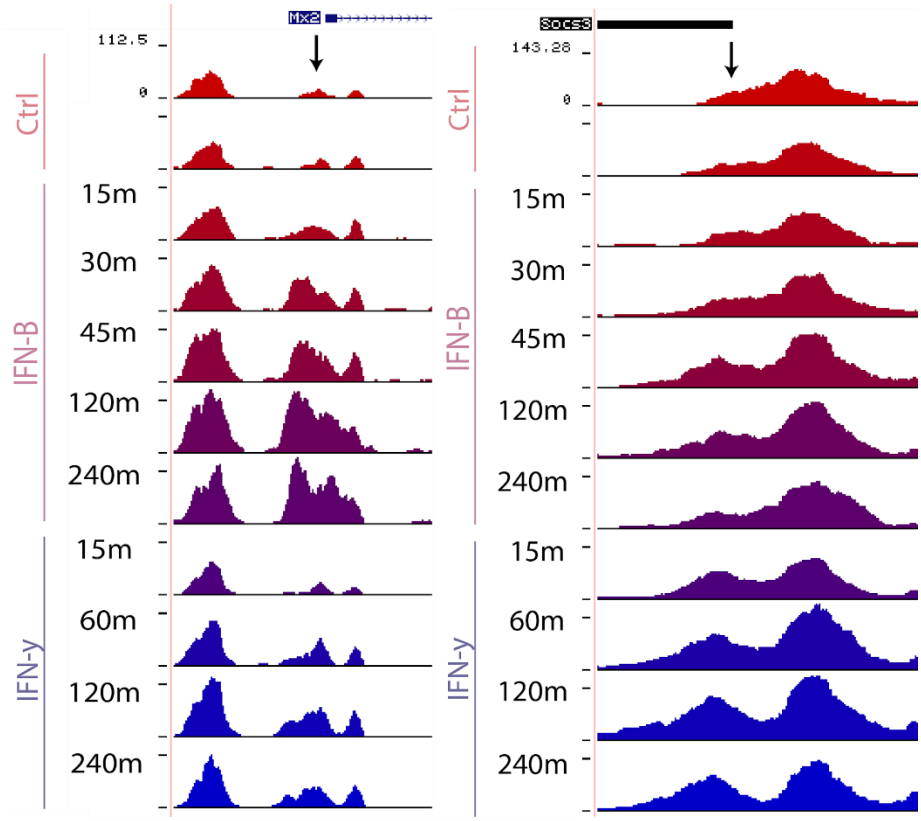


**Figure 8: Changes in ATAC-seq peaks reflect TSR activity in csRNA-seq.** Location of TSR determined by csRNA-seq is denoted by a black arrow.

In Figure 8 the changes in chromatin accessibility correlate with increased transcriptional activity seen previously in the RNA-seq and csRNA-seq data. For example, the gene Mx2 is upregulated by both Type I and Type II IFN but is significantly more induced by Type I, owing to its involvement in the strong antiviral response associated with Type I IFN. ATAC-seq peaks show open chromatin increases broadly around the Mx2 promoter, but at the TSR the increase is

more specific to IFN-β and occurs more rapidly. A similar dynamic is displayed in IFN-γ specific genes such as SOCS3, where the increase in chromatin accessibility around the start site is more marked in the IFN-γ treatment. Here, the change of topography of open chromatin peaks is clear; in the non-treatment control sample there is one broad peak centered upstream of SOCS3, but in the IFN-γ treatment samples (and later timepoints for IFN-β treatment) we see a new distinct peak emerge around the TSR.

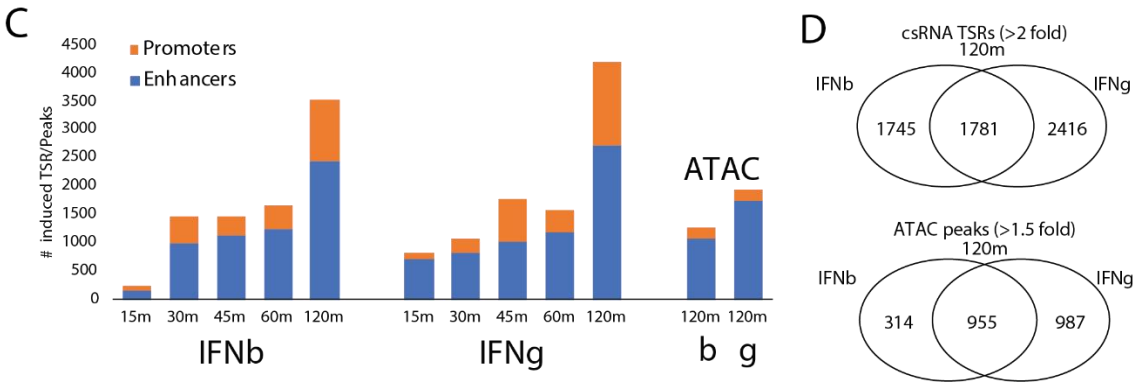


**Figure 9: Characterization of Promoter and Enhancer Prevalence in TSR peaks.** Promoter distal regions were defined as TSR located at least 500 bp away from the nearest defined promoter regions.

In order to determine the sequence-specific patterns that underly IFN-I specific signaling, we sought out to identify differentially regulated enhancers and promoters from the TSR peaks. Significantly more enhancers were identified compared to promoters as shown in Figure 9 panel C, and the number of induced cis-regulatory elements identified generally increased over the time course experiment. The csRNA-seq method is generally more sensitive, identifying more significantly upregulated TSRs compared to ATAC-seq. Visual inspection of the browser data shows that many of the TSRs identified by csRNA-seq correspond to regions of chromatin that remain open in all ATAC-seq samples, including the control, untreated samples. Therefore, many of these significant cis-regulatory elements would not have been identified from ATAC-seq data alone. The significant degree of overlap between IFN-β and IFN-y targets is also shown in Figure 9 Panel D.

## 2.2 Analysis of DNA Motifs in Interferon Regulatory Elements

I first found TSR peaks in each sample relative to its input to correct for highly prevalent non-capped RNA species, then merged the peaks across treatments for each timepoint. Next I determined which peaks were differentially expressed by comparing each treatment to the background non-treatment control across the merged set of peaks. I then did motif finding with HOMER using the set of peaks enriched in the treatment relative to background. Below in Figure 10 is the motif finding results in peaks enriched in the IFN-β treatment relative to IFN-γ at the 30m time point. The interferon-stimulated response element (ISRE) was the most enriched motif, and the T1ISRE was among the similar motifs found in 10.86% of targets.

| Rank | Motif | P-value | log P-pvalue | % of Targets | % of Background | STD(Bg STD) | Best Match/Details |
|---|---|---|---|---|---|---|---|
| 1 | | 1e-80 | -1.853e+02 | 8.71% | 1.45% | 72.0bp (116.5bp) | IRF3(IRF)/BMDM-Irf3-ChIP-Seq(GSE67343)/Homer(0.993) More Information \| Similar Motifs Found |
| 2 | | 1e-42 | -9.765e+01 | 1.33% | 0.02% | 54.9bp (103.2bp) | PB0134.1_Hnf4a_2/Jaspar(0.631) More Information \| Similar Motifs Found |
| 3 | | 1e-27 | -6.365e+01 | 0.95% | 0.02% | 25.8bp (122.5bp) | PB0194.1_Zbtb12_2/Jaspar(0.651) More Information \| Similar Motifs Found |
| 4 | | 1e-20 | -4.641e+01 | 0.48% | 0.00% | 47.1bp (0.0bp) | PB0152.1_Nkx3-1_2/Jaspar(0.655) More Information \| Similar Motifs Found |
| 5 | | 1e-17 | -4.097e+01 | 0.43% | 0.00% | 2.8bp (0.0bp) | HNF4A(var.2)/MA1494.1/Jaspar(0.557) More Information \| Similar Motifs Found |
| 6 | | 1e-17 | -4.097e+01 | 0.43% | 0.00% | 108.5bp (0.0bp) | NR4A2/MA0160.1/Jaspar(0.713) More Information \| Similar Motifs Found |
| 7 | | 1e-16 | -3.819e+01 | 0.62% | 0.02% | 76.9bp (88.6bp) | ZBTB12/MA1649.1/Jaspar(0.609) More Information \| Similar Motifs Found |

| Rank | Match Score | Redundant Motif | P-value | log P-value | % of Targets | % of Background |
|---|---|---|---|---|---|---|
| 1 | 0.902 | | 1e-42 | -97.242048 | 15.05% | 6.51% |
| 2 | 0.815 | | 1e-31 | -72.547147 | 10.86% | 4.58% |

**Figure 10: Motif Finding for Interferon Regulatory Elements.** ISRE motif was the highest ranked motif using HOMER. Analysis of similar motifs showed the T1ISRE was the closest in rank.

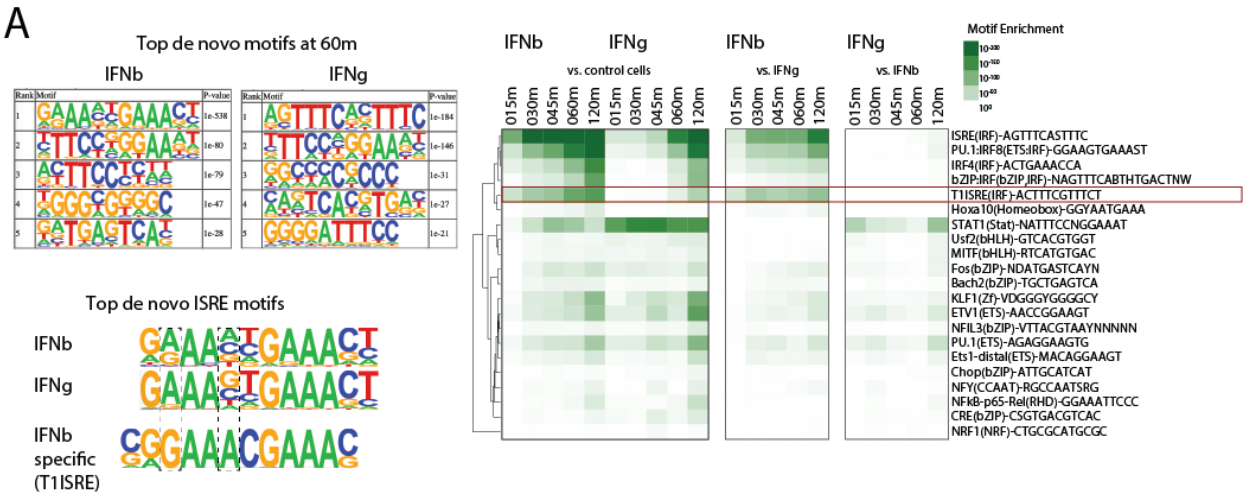


**Figure 11: De novo Motif Finding at 60-minute Timepoint and Clustering Analysis.** Left panel shows top de novo motifs at the 60m treatment timepoint for IFN-β and IFN-γ. Right panel is a heatmap of top enriched motifs after clustering, T1ISRE motif outlined by the red box.

Analysis of the 60m timepoint showed the ISRE is again the most prevalent motif; the motif nucleotide preferences for IFN-β versus IFN-γ shows that the IFN-β ISRE has more variability at nucleotide positions 2 and 5 corresponding to the compressed T1ISRE, this pattern is further illustrated at the bottom left. Type II IFN is preferentially enriched for GAS elements. On the right is a clustering heatmap of top enriched motifs at each timepoint. T1ISRE is present and displays selective enrichment in IFN-β treatment samples compared to IFN-γ, this selectivity is visible early on at the 15-minute time point. Additionally, it displays higher enrichment at earlier time points compared to motifs that may be more prevalent overall in the IFN-β stimulated macrophages compared to the controls. Type II is preferentially enriched for GAS elements while Type I is preferentially enriched for a version of the ISRE that is 'condensed' (GAAAnGAAA). This is also reflected in a 'composite' ISRE found by de novo motif finding when analyzing IFN-β induced sites.

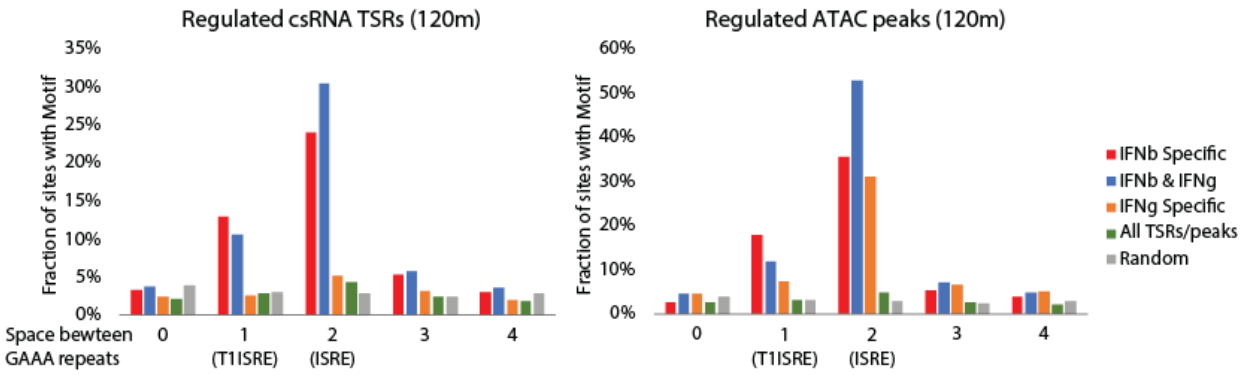


**Figure 12: Preferential spacing between GAAA repeats in csRNA-seq and ATAC-seq defined TSRs.** 0: GAAAGAAA, 1: GAAANGAAA (T1ISRE), 2: GAAANNGAAA (ISRE), 3: GAAANNNGAAA, 4: GAAANNNNGAAA

To evaluate the broader effects of spacing between the GAAA repeats present in the ISRE motif (also the IRF element), an unbiased comparison of spacing possibilities was done at differentially enriched csRNA-seq and ATAC-seq peaks. Peaks were classified by their log 2-fold change as either IFN-β specific, IFN-γ specific, IFN-β and IFN-γ upregulated, nonspecific, or random. csRNA-seq peaks and ATAC-seq peaks displayed similar patterns of spacing preference. The 1 nucleotide spacing between GAAA repeats corresponding to the T1ISRE sequence was the most prevalent in IFN-β-specific peaks for both csRNA-seq and ATAC-seq, while the ISRE was more prevalent in IFN-β and IFN-γ responsive peaks. Other spacing schema were significantly less frequent and specific.

The T1ISRE is present in the promoters and/or enhancers of several type I-specific genes including those directly involved in strong antiviral responses such as Mx1, Mx2, ADAR, and Trim30c. Murine Trim30c is homologous to human Trim5, which prevents infection from certain retroviruses (Ozato et al., 2008) and substitutions of two amino acids is sufficient to confer protection against HIV-1 (Dufour et al., 2018). The wildtype form of Mx2 inhibits HIV-1 replication and the broader Type I IFN-induced response to HIV-1 is significantly attenuated by its depletion (Kane et al., 2013). Mx1, a paralog of Mx2 also

contains a T1ISRE in its promoter and is a critical inhibitor of influenza viruses including the highly lethal 1918 and H5N1 strains (Tumpey et al., 2007). ADAR has an identical T1ISRE motif shared by STAT1 (Dansako et al., 2003).

### 2.3 T1ISRE is preferentially bound by ISGF3 complex

I next compared my experimental findings with ChIP-seq data generated in primary mouse macrophages (reference PMID:31266943). Chromatin Immunoprecipitation and sequencing (ChIP-seq) is used to find regions of DNA bound by a chromatin associated protein -often a transcription factor- of interest genome wide, by precipitating with a protein-specific antibody. The proteins are removed, and the previously bound DNA is sequenced to determine the location in the genome and any sequence-specific features.

| ChIP | ISRE | T1ISRE | GAS |
|---|---|---|---|
| BMDM-Irf9-ctrl | 33% | 44% | 11% |
| BMDM-Irf9-IFNb-90m | 89% | 91% | 64% |
| BMDM-Irf9-IFNg-90m | 80% | 85% | 67% |
| BMDM-Stat1-ctrl | 3% | 3% | 1% |
| BMDM-Stat1-IFNb-90m | 71% | 80% | 74% |
| BMDM-Stat1-IFNg-90m | 50% | 59% | 76% |
| BMDM-Stat2-ctrl | 26% | 40% | 10% |
| BMDM-Stat2-IFNb-90m | 85% | 91% | 70% |
| BMDM-Stat2-IFNg-90m | 66% | 78% | 51% |

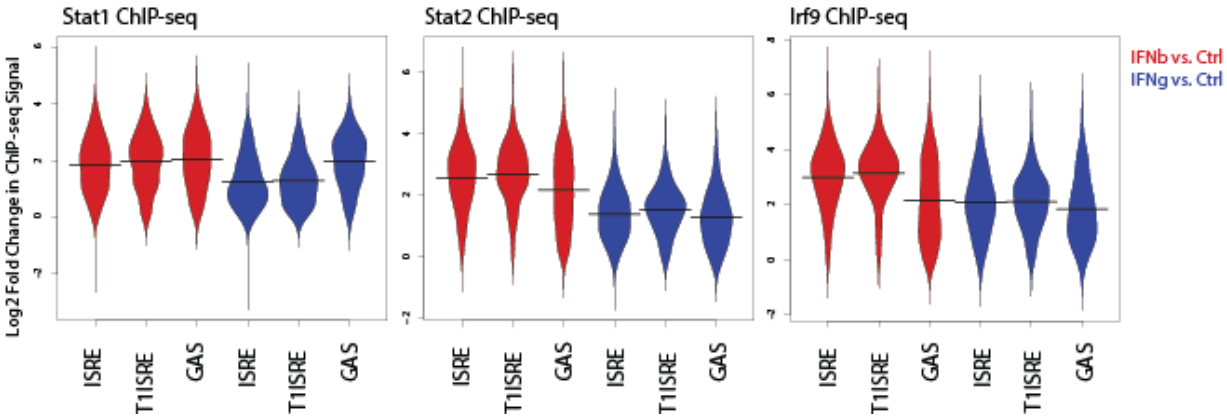


**Figure 13: Preliminary ChIP data of ISGF3 components overlaps with csRNA-seq peaks enriched for ISRE, T1ISRE, and GAS.** Top: table showing the percentage of motifs in csRNA-seq identified peaks that overlap with ChIP-seq peaks for each experiment (first column). Bottom: violin plots log2 fold changes in ChIP-seq signal at each motif after stimulation with IFN-β or IFN-γ.

Some expected trends are visible, such as the significant occupation of all components making up the ISGF3 complex (Irf9, STAT1, STAT2) at the ISRE when stimulated by IFN-β. Additionally the binding of these factors increases after both IFN-β and IFN-γ treatment compared to the controls, further illustrating the overlap between pathways. Also as expected the increase of STAT1 binding was most pronounced after treatment of IFN-γ at GAS elements. Interestingly the T1ISRE motif had the greatest log 2-fold change in signal for all transcription factors after IFN-β treatment, a slightly larger increase than that at the ISRE motif.

The preference of the ISGF3 complex for the T1ISRE and ISRE was investigated by Electrophoretic Mobility Assay, preliminary data collected by Dr. Chris Benner for his dissertation. Here RAW264.7 cells were treated either with IFN-β, IFN-γ, or LPS (lipopolysaccharide) another strong activator of macrophages.

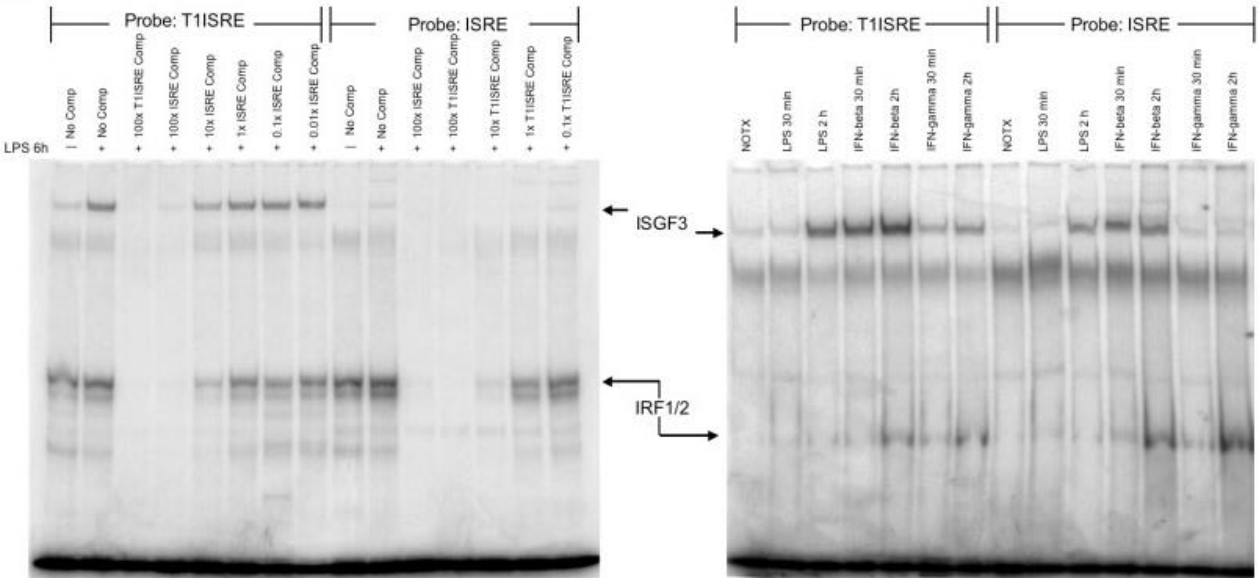


**Figure 14: Preliminary EMSA data collected by advisor Dr. Chris Benner.** Left: competitive EMSA after stimulating with LPS. Right: stimulation with either LPS, IFN-β, or IFN-γ for 30m and 2 hr.

The left panel shows competitive EMSA after LPS stimulation, where the T1ISRE probe is bound more competitively by ISGF3 than by the ISRE probe. The T1ISRE is more

specific to the ISGF3 complex, while IRF1/2 dimers are not specific as evidenced by their similar band intensities in both ISRE and T1ISRE probed samples with and without competition. The right panel compares different stimulation methods (LPS, IFN-β and IFN-γ) as well as various incubation times. The pronounced bands visualized with the T1ISRE probe at 30m and 2h after IFN-β stimulation show a more rapid response compared to both LPS and IFN-γ.

# 3 Discussion

## 3.1 Summary

To better understand Type I vs Type II IFN responses, I examined the composition of regulatory elements specific to each pathway. I used csRNA-seq to capture short capped RNAs and identify transcriptional start regions (TSRs) in both promoters and enhancers at base-pair resolution. I applied this method to analyze the transcriptional responses in RAW264.7 murine macrophage-like cells responding to a time course of stimulation with Type I and Type II Interferon (IFN). I classified differentially regulated promoters and enhancers based on csRNA-seq-enabled identification of these TSRs and supporting ATAC-seq and ChIP-seq data. The time course of stimulation over 4 hours allowed visualization of the temporal dynamics of IFN signaling. I identified a novel variation of the classical Type I IFN DNA motif, the Interferon Stimulated Response Element (ISRE), called the Type I Interferon Response Element (T1ISRE). The T1ISRE is enriched in the promoters and enhancers of genes preferentially regulated by Type I IFN compared to Type II IFN.

## 3.2 Quantifying the Selectivity of the T1ISRE with a Luciferase Reporter Assay

I have ongoing experiments focused on isolating the T1ISRE motif's effect on IFN-I regulation. Luciferase reporter assays are a well-documented way to quantitatively compare the activities of regulatory elements. Candidate regulatory elements are cloned in either immediately upstream of a luciferase gene (for a candidate promoter) or further upstream or downstream for a candidate enhancer. I have constructed a series of reporter plasmids based on the TALp-pGRA1-βC+TA plasmid from Dr. Sven Heinz in the Benner and Heinz lab.

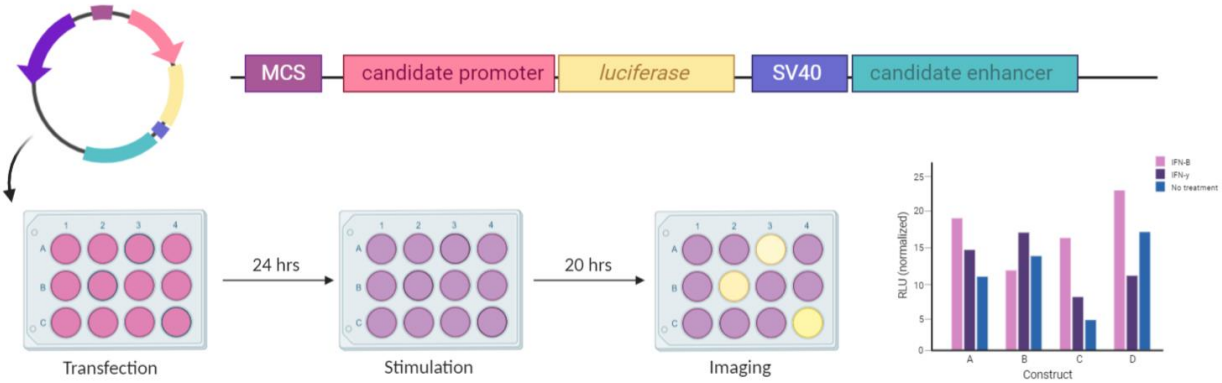


**Figure 15: Plasmid map of the TALp-pGRA1-βC+TA reporter plasmid and schematic of the luciferase reporter assay.** See additional details in Materials in Methods

The plasmid TALp-pGRA1-βC+TA is a pGL4.10 derived reporter, containing a TATA-like promoter from pTAL-luc, luc2 luciferase, and a downstream site for enhancer cloning (full map in Figure 16). All promoter constructs were cloned to replace the TATA-like promoter, all enhancer constructs were cloned downstream of the luciferase gene. The candidate promoters and enhancers were selected based on several criteria. First, each candidate must regulate a gene with observable differential expression based on my RNA-seq and csRNA-seq data, the log2 fold change for genes upregulated by each treatment was calculated from the 2-hour timepoint:

**Table 2: Rationalization for Selection of Native Promoter/Enhancer Constructs.** L2FC indicates the normalized log2 fold change in tag counts compared to the nontreatment control. UCSC Browser Coordinates reference the mm10 genome.

| Type | Gene source | Motif | IFN-β L2FC | IFN-γ L2FC | UCSC Browser Coordinates |
|---|---|---|---|---|---|
| Promoter | Oas3 | T1ISRE/ISRE | 2.340 | 1.002 | chr5: 120,777,520-120,777,850 |
| Promoter | Mx2 | ISRE/T1ISRE | 3.071 | 2.140 | chr16: 97,535,100-97,535,410 |
| Promoter | Trim30c | T1ISRE | 3.330 | 0.922 | chr7: 104,400,646-104,401,019 |
| Promoter | Tap1 | ISRE | 3.479 | 2.831 | chr17: 34,187,546-34,187,919 |
| Promoter | Slfn9 | ISRE | 2.936 | 3.256 | chr11: 82,991,646-82,992,019 |
| Promoter | CD14 | GAS | 0.395 | 0.217 | chr18: 36,726,508-36,726,881 |
| Promoter | Tgfbr1 | Sp1 | 0.884 | 0.347 | chr4: 47,353,050-47,353,310 |
| Enhancer | ADAR | T1ISRE | 3.092 | 1.094 | chr3: 89,730,642-89,730,847 |
| Enhancer | Synj1 | T1ISRE | 3.027 | 1.056 | chr16: 91,002,268-91,002,641 |
| Enhancer | Ppp2r5c | ISRE | 2.305 | 2.105 | chr12: 110,498,515-110,498,888 |
| Enhancer | Tbl2 | GAS | 1.300 | 2.980 | chr5: 135,145,574-135,145,947 |

Genes upregulated by either IFN-β, IFN-γ, or both that also contained the DNA binding motifs of interest were selected and displayed in Table 2. Of the genes responsive to IFN-β, multiple were selected in order to include those with an ISRE, T1ISRE, or both in their respective regulatory elements. Elements containing a GAS site were also selected as a control to monitor response to IFN-y. The Tgfbr1 promoter was used as a positive control as it contains a SP1 site. We also selected genes that were already known to be heavily involved in the IFN pathway corresponding to the type of IFN they respond to. To see the specific effects of the motifs of interest compared to the remainder of regulatory element structure, I generated mutated constructs with nonfunctional versions of each motif, displayed in Table 3.

**Table 3: Mutated Promoters.** Mutated promoters were generated by primer mutagenesis or E-βlock cloning (see Methods). Bolded sequences are the motif of interest, and the mutations created are in blue. The Mx2 promoter contains overlapping ISRE and T1ISRE motifs, mutated either separately or together in each construct as specified.

| Type | Gene source | Mutated Motif | Sequence of Interest |
|---|---|---|---|
| Mutated promoter | Tap1 | ISRE | ...GTCGG**CATACGGTTTC**TTCTT... |
| Mutated promoter | Slfn9 | ISRE | ...GAGCA**GATACGTTTTC**CCAAA... |
| Mutated promoter | Trim30c | T1ISRE | ...CAAGA**GCTCTGAAAG**TTAA... |
| Mutated promoter | ADAR | T1ISRE | ...TCAAG**GCTGCGAAAG**TGAAC... |
| Mutated promoter | Oas3 | T1ISRE and ISRE | ...GA**CAAAACGTAG**GT...GA**CAAACGTAG**CT... |
| Mutated promoter | Mx2 | T1ISRE and ISRE | ...CCAGA**GCTGTGACAGTGAAA**CTAAG... |
| Mutated promoter | Mx2 | T1ISRE | ...CCAGA**CTAGTGAAAGTGAAA**CTAAG... |
| Mutated promoter | Mx2 | ISRE | ...CCAGA**GAAATGAAAGTCTAG**CTAAG... |
| Mutated promoter | CD14 | GAS | ...TGCAA**TATTTACTCCCAG**TGAGT... |
| Mutated promoter | Tgfbr1 | SP1 | ...CCGC**AAGCGG**GGC...CGC**AAGCGG**CGGG... |

Next I selected constructs of promoters and enhancers that contained either the ISRE or T1ISRE motif and mutated them specifically to create the other motif of interest (i.e. a deletion was made in an ISRE sequence to create a T1ISRE motif, or an insertion was made in a T1ISRE motif to create an ISRE). The selected sequences are shown below in Table 4.

**Table 4: Swapped promoters/enhancers.** Insertions marked by blue nucleotide, deletions in spacing between GAAA repeats shown underlined.

| Type | Gene source | Motif | Sequence of Interest |
|---|---|---|---|
| Swapped promoter | Trim30c | T1ISRE → ISRE | ..GA**GAAATGAAA**GT..→..GA**GAAACTGAAA**GTT.. |
| Swapped promoter | Tap1 | ISRE → T1ISRE | ..GC**TTTCGGTTTC**TT.. → ..GC**TTTCGTTTC**TT.. |
| Swapped enhancer | ADAR | T1ISRE → ISRE | ..AG**GAAACGAAA**GT.. → ..AG**GAAACTGAAA**GT.. |
| Swapped enhancer | Ppp2r5c | ISRE → T1ISRE | ..AC**TTTCAGTTTC**TT.. → ..AC**TTTCGTTTC**TT.. |

Finally, I designed a set of synthetic promoters shown in Table 5, all identical except for the motif sequence of interest. Each synthetic promoter consists of a random sequence designed to minimize potential transcription factor binding with the motif of interest inserted at equally spaced intervals of 51 nucleotides following helical periodicity of ~10.2 Å.

**Table 5: Synthetic promoters.** Synthetic constructs consist of a random sequence interspersed with five equally spaced motifs of interest, followed by the beta-actin initiation sequence. Synthetic control contains the random sequence without motif insertions, the beta-actin initiation sequence is in bold.

| Name | Motif spacing | Motif | Sequence Structure |
|---|---|---|---|
| Syn_T1ISRE_51 | 51 bp | T1ISRE | ...**T1ISRE**...**T1ISRE**...**T1ISRE**...**T1ISRE**...**T1ISRE**...ActB Initiator |
| Syn_ISRE_51 | 51 bp | ISRE | ...**ISRE**...**ISRE**...**ISRE**...**ISRE**...**ISRE**...ActB Initiator |
| Syn_GAS_51 | 51 bp | GAS | ...**GAS**...**GAS**...**GAS**...**GAS**...**GAS**...ActB Initiator |
| Syn_SP1_51 | 51 bp | SP1 | ...**SP1**...**SP1**...**SP1**...**SP1**...**SP1**...ActB Initiator |
| Syn_control | N/A | None | TCTCAGCGCCCGATCAGTCAACGCAGTGCGTGCGTAGGTAACTCTTTGTCGGTGATCTAGCGCTTGCGTTCTTAGGTACCATCTAGATGGCCCCTCCGAACGACCAACTCCCCTCGAGACGTCG**AGGCTCGAGTGGCCGCTGTGGCGTCCTATAAAACCCGGCGGCGCAACGC** |

These constructs were created and transfected into RAW264.7 cells as specified in the Materials and Methods section. Assaying the luciferase output from each at various timepoints after IFN-β or IFN-γ stimulation will be done as another confirmation of the specificity conferred by the T1ISRE. Testing whether a promoter with an ISRE will become more responsive to IFN-β when the motif is changed to a T1ISRE is of great interest. Testing each native promoter and enhancer along with a version of each with the specific motif of interest mutated allows us to separate the effect of the motif from the surrounding regulatory architecture.

### 3.3 Similar Regulatory Models in Literature

The proposed model of regulatory specificity arising from small differences in motif spacing occurs in other regulatory elements. For example, the AP1 binding motif 5'-TGANTCA-3' is nearly identical to the CREB binding motif 5'-TGANNTCA-3' with only a difference in spacing between the repetitive palindromic elements. Additionally, the preferred STAT6 binding motif 5'-TTTCNNNNGAAA-3' has an additional nucleotide in the space between its recognition sequences compared to the STAT1 motif 5'-TTTCNNNGAAA-3'. There is also evidence of ISRE variants in literature, a 5'-extended ISRE was recently discovered to be more specific to IFN- γ, and was crucial for Type II IFN-induced upregulation of TRIM22 (Gao et al., 2010).

### 3.4 Future Study

Given that the T1ISRE appears to be more specific to Type I IFN, the next step is to investigate the sequence conservation of T1ISRE across mammalian genomes. General conservation in gene paralogs across species would indicate that the T1ISRE is a distinct response element. In addition, there is currently anecdotal evidence that the T1ISRE tends to be conserved both across gene families in the same organism and for similar gene families in different species (i.e. both Mx1 and Mx, and human Oas1 and mouse Oas3 have the T1ISRE motif). However, the mouse homologs to Oas1 contain an ISRE. In mice the Oas isoforms originate from gene duplication while in humans they arise from alternative splicing, so conducting an unbiased search for the T1ISRE across species and gene families would help gain an understanding of how the motif evolved (Pulit-Penaloza et al., 2012). Functional conservation of regulatory elements in homologous DNA where the same element evolves to control the same genes independently would provide additional support that the regulatory elements serve important purposes. We would also investigate whether genes harboring

T1ISRE vs. ISRE maintain their specificity throughout evolution (greater than expected by chance). During my preliminary analysis I discovered a T1ISRE in zebrafish, if more analysis was done across species the evolutionary history of T1ISRE evolution could help determine if the T1ISRE evolved as a way to confer specificity between Type I and Type II IFN around the time IFN-II evolved. Evidence of human genetic variation that affecting the selectivity of Type I and Type II responses would be another confirmation, as a difference in IFN specificity would likely have some phenotypic effect, as improper IFN regulation has been implicated in multiple diseases.

# 4 Materials and Methods

## 4.1 Cell culture and treatment

RAW264.7 cells were cultured in RPMI-1640 (Thermo Fisher 21870076) +10% heat-inactivated FBS, +1% Glutamax, +1% Penicillin/Streptomycin. Cells were thawed within 2 weeks of stimulation, and no more than 3 passages were done to reduce the likelihood of genetic drift. The day before stimulation, 10cm and 6cm plates were seeded with 3.3e6 and 1.2e6 cells, respectively. Mouse IFN-β (R&D Systems, Lot #DCUU0519061) was reconstituted at 1e6 IU/mL (1000x the final working dilution) in PBS + 0.5% endotoxin-free BSA. Mouse IFN-γ (R&D Systems, Lot #CFP2819111) was reconstituted at 10ug/mL (1000x the final working dilution) in PBS + 0.5% endotoxin-free BSA. Aliquots stored at -80°C. IFN-β was added to cells at a final concentration of 1000 IU/mL, IFN-γ and IFN-λ were added to cells at a final concentration of 10ng/mL.

## 4.2 Nuclear RNA Extraction

At the appropriate time point, cells were shock-cooled with cold PBS and immediately placed on ice. Cells were washed 2x more with cold PBS, then scraped with cold PBS + 10% glycerol and transferred to pre-chilled 15mL Falcon tubes. Cells were centrifuged at 400g, 4°C for 10 minutes, supernatant was discarded. The pellet was resuspended in 700µL Swelling Buffer + 10% glycerol; then Lysis Buffer (Swelling Buffer + 1% IPEGAL) was added dropwise while slowly vortexing, tube was incubated on ice for 5 minutes. Lysate was transferred to a 1.5mL RNase/DNase free tube (VWR 89082-332), nuclei pelleted at 600g, 4°C for 8 minutes, supernatant discarded. Pellet washed with 500µL Wash Buffer (50:50 of Swelling and Lysis Buffer, final IPEGAL 0.5%), then underlaid with Freezing Buffer and spun at 800g, 4°C for 10 minutes. Supernatant was removed carefully from top to bottom to ensure

Wash Buffer was completely removed, then pellet resuspended in 200µL Freezing Buffer, and nuclei counted. Approximately 250k nuclei were reserved for ATAC-seq, the remaining sample was used for csRNA-seq.

### 4.3 ATAC-seq

A master mix was prepared with 25µL of 2x DMF, 2µL Tn5, and Freezing Buffer was added to a final volume of 50µL (including volume of nuclei in Freezing Buffer). 2x DMF diluted with Freezing Buffer first to avoid inactivation of Tn5. Samples were incubated at 37°C for 30', then purified with Zymo ChIP DNA Clean & Concentrator Kit (Genesee Scientific 11-379C), eluted 2x in 9µL ATAC Elution Buffer (10mM Tris-HCl pH 8.0 + 0.05% Tween). Samples PCR amplified with TruSeq barcodes, 0.5M Betaine, and Q5 polymerase for 11 cycles. PCR products were loaded with 1x DNA loading buffer and run on a 10% TBE gel (EC62752BOX) at 80V for 15' then 180V for 70'. The gel was stained with CybrGold and cut from 160-250 bp, gel piece was sliced with a p10 pipette, and eluted with ATAC Elution Buffer overnight at room temperature. The Zymo ChIP DNA Clean & Concentrator Kit was used to concentrate the samples, then they were eluted in 30 µL of 70°C Sequencing TE'T. Samples were quantified with Qubit HS dsDNA Kit, pooled, and sequenced.

### 4.4 csRNA-seq

#### 4.4.1 RNA Precipitation

750µL of Trizol LS (Life Technologies 10296028) was added to the remaining nuclei in Freezing Buffer, sample was vortexed well, 200µL of $CHCl_3$ (Sigma-Aldrich C0549-1PT), the sample was vortexed well then spun down for 10 minutes at 12,000g, 4°C. The top layer was carefully transferred to a new tube and 1/10 volume of 3M NaOAc was added. The tube was vortexed well, then 1 volume of isopropanol (I9516-25mL) and 1.5µL glycoblue (Fisher Scientific AM9516) were added; the tube was again vortexed well, then the RNA was

precipitated at -20°C overnight. The RNA was pelleted at >20,000g for 30’ at 4°C, the supernatant was removed, and the pellet was washed with 70% ethanol and dried at room temperature. The RNA pellet was resuspended in 20µL TE’T and quantified using a Nanodrop.

### 4.4.2 RNA Size Selection

A 15% TBE-Urea gel (Life Technologies EC6885BOX) was pre-run for 30 minutes at 200V in 1xTBE running buffer. 10ug of RNA per sample was mixed with equal volume of Formaldehyde Loading Buffer, and RNA was denatured by heating to 75°C for 3’, then chilled on ice. The gel wells were flushed out with 1x TBE buffer using a 20-gauge needle immediately before loading the samples, then the gel was run for 40 minutes at 200V, until the lower dye band of bromophenol blue was ¼ from the bottom of the gel. The gel was stained with 0.5ug/mL GelGreen (Fisher Scientific 41004), then the portion of the gel corresponding to 15-60nt length RNA was excised. The gel slice was placed in a Qubit tube nested inside a 1.7mL LowBind tube, the Qubit tube having 3 holes made from a 22g needle. The nested tubes are then spun down at >20,000g for 5 minutes to shred the gel slices into the bottom of the outer tube. The shredded gel slices were eluted in 300 µl START EB on a shaker for 3 hours. The gel slurry is then transferred with a wide-βore tip (VWR46620-642) to a spin column (UltraFree MC, 0.45 µm, Millipore UFC30HVNB) placed inside a Lowbind tube. 1.5µL glycoblue and 2.5x Vol of EtOH were added, the tube was vortexed, and stored at -80°C overnight.

### 4.4.3 5’ Cap Enrichment

Samples were then spun down at >20,000g, 30 minutes, 4°C, then the pellet was washed with 75% EtOH, transferred to an 8-strip PCR tube and air dried for 5 minutes. The RNA pellet was resuspended in 6µL TE’T and denatured at 75°C for 3 minutes then immediately placed back on ice. 0.5µL of each sample was removed and kept for the input control (input samples were added back for library preparation). 14µL of Terminator Master Mix was added to each

sample, then samples were incubated at 30°C for 1 hour. Next 30µL of CIP Master Mix was added to the samples and incubated at 37°C for 45 minutes. Samples were purified by adding 1 volume (50µL) of RNA XP Beads (Beckman Coulter A63987) and 1 volume of isopropanol (100µL), vortexing, incubating on ice for 10 minutes, then collecting the beads on a magnet, washing 2x in 80% EtOH + 0.05% Tween, and eluting in 20µL TET. Samples were once again heated to 75°C for 3 minutes, then immediately placed on ice. 30µL of CIP Master Mix was added, and samples were incubated at 37°C for 30 minutes. 100µL of TE'T was added, then beads were collected on a magnet and the liquid remaining was transferred to a clean Lobind tube. 500µL of Trizol LS was added to the tube, then the sample was vortexed, and vortexed again after adding 150µL chloroform. Trizol extraction was performed as specified in the RNA Precipitation section. After precipitating RNA at -20°C, samples were once again spun down at >20000g, 4°C, for 30 minutes, then washed with 75% EtOH and dried.

### 4.4.4 Library Preparation

RNA pellets were dissolved in 3µL of TE'T and denatured at 75°C for 90 seconds. Input samples were added for the remainder of the protocol. 5µL of MM1 was added to the PCR strip lids, then the samples were mixed vigorously and spun down multiple times to ensure proper mixing of the PEG8000. MM1 reaction was carried out at 37°C for 90 minutes. Next 4µL of MM2 was added to each sample, mixed well and spun down, then incubated at 22°C for 2 hours. Reverse transcription primer hybridization was done by adding 1µL of 5uM RT primer and incubating for 75C for 2 minutes, then 37°C for 20 minutes, 25°C for 15 minutes, and holding at 4°C. The 5' adapter was ligated by adding 4µL of MM3 to the samples, mixing well and spinning down, then incubating at 25°C for 1 hour. 5.25µL of the Reverse transcription reaction mix (MM4) was added, then tubes were incubated at 50°C for 1 hour, then holding on ice. The samples were then barcoded by adding the PCR Barcoding MM, then amplified with

the following protocol:

94°C for 3 minutes
12 cycles of:
94°C for 45 seconds
63°C for 30 seconds
70°C for 15 seconds
72°C for 5 minutes

### 4.4.5 Bead Size Selection/Gel Purification

Added 1.5 volumes (86µL) of SpeedBeads Mix (3uL SpeedBeads, 41.5µL 40% PEG8000, 41.5µL 5M NaCl), then vortexed and incubated on ice for 10 minutes. Beads were collected on a magnet, then the supernatant was discarded and beads were washed 2x with 200µL 80% EtOH, then dried well ensuring no ethanol remained. DNA was eluted in 1x Loading Buffer (5x Novex HiDensity TBE Buffer Invitrogen LC6678 diluted 1:5 in H2O). Samples were run adjacent to their corresponding inputs on a 12-well 10% TBE gel (Life Technologies EC62752BOX), along with 25bp ladder (Invitrogen 10488-022) for 15 minutes at 80 volts then 75 minutes at 180 volts, until the upper band of dye (xylene cyanole) was within 1 cm from the bottom of the gel. Gel was stained with 1µL Cybr Gold in 10mL TBE buffer, then visualized with UV. Gel was cut from 140-175bp as demonstrated in Supplemental Materials, care was taken to ensure all bands of steady-state RNA and adapter dimers were avoided and that samples were cut identically to their corresponding inputs. Gel slices were split in half with a pipette tip then eluted in 150µL of Gel Elution Buffer overnight at room temperature. 750µL of Zymo ChIP DNA Binding Buffer was added, then samples were transferred to Zymo Spin Columns and purified according to the Zymo DNA Clean and Concentrator kit until the elution step. Samples were eluted in 20µL Sequencing TET that was prewarmed to 70°C in a water bath, inputs were eluted in 40µL. Samples and input concentrations were determined by Qubit Fluorometric Quantification using the dsDNA High Sensitivity kit (Thermo Fisher Cat

Q32851), then pooled and sequenced.

### 4.5 Luciferase Reporter Assay Cloning

#### 4.5.1 Cloning Native Promoters and Enhancers from RAW264.7 Macrophages

To isolate genomic DNA from a freezing vial in DMSO/FBS/RPMI, one vial of cells was thawed in a 37°C water bath until a small piece of ice remained in the vial, then the vial was quickly transferred to tissue culture hood and RAW264.7 cell media (RPMI + 10%FBS + 1x Glutamax + 1% Penicillin/Streptomycin) was added dropwise to vial, then the vial contents were transferred to sterile 15mL Falcon tube and more media added dropwise to 5mL. Cells were centrifuged at 1000g for 5 minutes, then supernatant was removed and the pellet was resuspended in 200µL of DNA extraction buffer and transferred to a clean 1.5mL tube. 1.5µL of 20mg/mL proteinase K was added to the lysate and incubated for 3 hours at 55°C. DNA was phenol/chloroform extracted by first adding 200µL H20, then adding an equal volume of phenol/chloroform/isoamyl alcohol (25:24:1, Invitrogen 15593031), vortexing well, then centrifuging at >20,000g for 10 minutes at room temperature. The upper layer was transferred to a new 1.5mL centrifuge tube, then 400µL chloroform was added and the tube was vortexed then centrifuged for 5 minutes at >20,000g, room temperature. The upper layer was transferred to a new 1.5mL centrifuge tube, then 1/10 volume of 3M NaOAc and 2.5 volumes of 100% EtOH were added. The tube was vortexed then incubated at -80°C for at least 1 hour. The tube was then centrifuged for 30 minutes at >20000g, room temperature, the supernatant was removed, and the pellet was washed with 75% EtOH and dried. Once the white pellet became glassy in appearance, 50µL of TE buffer was added and the DNA was quantified using a Nanodrop. Native promoters and enhancers of interest were amplified from the genomic DNA. Each PCR reaction was done with 25ng of genomic DNA, 0.3 nmol of each primer, 1x Q5 Mastermix (NEB M0492L), and 2M Betaine (Sigma Aldrich B0300) to a final volume of

50µL, then split into 5 reactions to optimize primer Tm (Tm: 52, 55, 58, 61, 65). All promoter and enhancer regions ranged from 300-400bp. The reactions were amplified with the following protocol:

98°C for 2 minutes
31 cycles:
98°C for 15 seconds
Gradient Tm for 20 seconds
72°C for 30 seconds
72°C for 3 minutes

The promoters and enhancers not successfully amplified by this protocol were amplified using 100ng genomic DNA, 0.3nmol of each primer, 1x Q5 Mastermix, and 0.5M Betaine. The Tm was raised to 68°C, the ramp rate was decreased to 1.5 °C/s, and the annealing time was increased to 45 seconds. PCR products were purified with the Zymo DNA Clean & Concentrator Kit (Zymo Research D4033). All promoter constructs were cloned into the NheI/HindIII site that replaces the TATA-like promoter; all enhancer constructs were cloned into the BamHI/SalI site downstream of the luciferase gene. Briefly, 1ug of plasmid DNA was digested with 20U each of the necessary restriction enzymes (NEB R3131, R3104, R0136, R0138) and 1x Cutsmart for 3 hours at 37°C, then purified with the Zymo DNA Clean & Concentrator kit. The amplified promoters/enhancers were annealed by Gibson reaction at a 2:1 molar ratio of insert to digested vector backbone using NEB 2x Hifi Ligation mix (NEB E2621), and incubated for 1 hour at 50°C. 5-alpha Competent E. coli (NEB C2987) were thawed on ice, then 0.7µL of the ligation reaction was added to 10µL of thawed bacteria. Bacteria were heat shocked at 42°C for 30 seconds then immediately placed on ice and 50µL of SOC Media (Thermo Fisher 15544034) was added to each reaction. Bacteria were plated on pre-warmed LB carbomycin plates and incubated for 16 hours at 37°C. Proper ligation was confirmed by colony PCR; three colonies from each plate were selected and added to 50µL of dH2O. Separately, the PCR reaction was made with 1x

Q5 master mix, 1M Betaine, and 0.3 nmol each of primers which amplify from upstream and downstream of the insertion site in the plasmid, then 5µL of the bacteria colony in water was added to 15µL of the PCR reaction mix, and amplified as follows:

98°C for 3 minutes
30 cycles of:
98°C for 15 seconds
62°C for 20 seconds
72°C for 30 seconds
72°C for 3 minutes

Colony PCR products were confirmed by Sanger sequencing, and the correct colonies were grown overnight, then purified using the PureLink HiPure Plasmid Midiprep Kit (Thermo Fisher K210004) to ensure the plasmids were free of LPS.

### 4.5.2 Cloning Synthetic Constructs

Synthetic constructs were ordered as E-βlocks through IDT, then resuspended in $H_2O$ and ligated into the BamHI/SalI digested reporter at a 2:1 molar ratio and transformed into 5-alpha Competent E. coli as described above. Colony PCR was performed for each construct, and sequence verified colonies were grown overnight in LB-amp cultures then plasmids were extracted using the PureLink HiPure Plasmid Midiprep Kit (Thermo Fisher K210004).

### 4.5.3 Primer Mutagenesis to Generate Mutated Constructs

Each mutated promoter or enhancer construct was created by amplifying the reporter containing the native sequence with primers that introduce substitution mutations in the particular motif of interest to render it inactive. 25ng of each template plasmid was amplified with 0.2nmol of each primer and amplified for 12 cycles with an extension time of 2 minutes and 30 seconds. The PCR reaction was then digested with 20U of DpnI (NEB R0176S) to remove the original plasmid with methylated 5’-GATC-3’. 5µL of the digested plasmid was then directly transformed into 20µL of NEB 5-alpha Competent E. coli (NEB #C2987) as described

previously. Colony PCR was performed, and plasmids were verified by Sanger sequencing.

### 4.6 NGS Data Analysis

**Table 6: NGS Analysis of csRNA-seq Data.**

| Purpose | command |
|---|---|
| FastQC | **fastqc** -o fastqcresults/ <file.fastq.gz> |
| Trimming sequencing reads at 3' end | **homerTools** trim -3 AGATCGGAAGAGCACACGTCT -mis 2 -minMatchLength 4 -min 20 <file.fastq.gz> |
| Generate Indexed Genome | **STAR** --runMode genomeGenerate --runThreadN 24 --genomeDir ./ --genomeFastaFiles genome.fa |
| Align sequences to Indexed Genome | **STAR** --genomeDir /home/lahodge/mm10/mm10-StarIndex/ --runThreadN 24 --readFilesIn </path/to/file.fastq.gz.trimmed> --outFileNamePrefix </path/to/filename> --outSAMstrandField intronMotif --outMultimapperOrder Random --outSAMmultNmax 1 --outFilterMultimapNmax 10000 --limitOutSAMoneReadBytes 10000000 |
| Create HOMER Tag Directories | **makeTagDirectory** samplename-tagDir/ samplename.Aligned.out.sam -genome mm10 -checkGC -fragLength 150 |
| Generate BedGraph Files | **makeUCSCfile** filename_csRNA-tagDir/ -style tss -strand + > samplename.posStrand.bedGraph<br>**makeUCSCfile** filename_csRNA-tagDir/ -style tss -strand - -neg > samplename.negStrand.bedGraph |
| Finding csRNAseq Peaks | **findPeaks** experiment-csRNA-tagDir/ -i experiment-input-tagDir/ -style tss > tssOutput.txt |
| Merging TSR Peaks | **mergePeaks** treatment1_timepointA_csRNA_tssOutput.txt treatment2_timepointA_csRNA_tssOutput.txt -strand > timepointA_Merged.tss.txt |
| Quantitatively Compare Experiments | **annotatePeaks.pl** timepointA_Merged.tss.txt mm10 -strand + -fragLength 1 -raw -d Controlsample-csRNA-tagDir/ treatment1_timepointA_csRNA- tagDir/ treatment2_timepointA_csRNA-tagDir/ > TimepointACounts.txt |
| Find Differentially Expressed Peaks between two experiments | **getDifferentialPeaks** <peak/BED file> <target tag-dir/> <background tag-dir/> [options] |
| XY Scatter Plot | **annotatePeaks.pl** TimepointA_treatmentCtrl_Merged.tss.txt mm10 -size -500,100 -strand + -fragLength 1 -d treatment1_csRNA-tagDir/ Control_csRNA -tagDir/ > TimepointA_Treatment1Ctrl_plot.txt |
| Annotated the peaks differentially expressed | **annotatePeaks.pl** TimepointA_treatmentCtrl_Diffpeaks.txt mm10 > annotated_timepointA_treatmentCtrl_Diffpeaks.txt |
| Motif Finding | **findMotifsGenome.pl** TimepointA_treatment1_treatment2_Diffpeaks.txt mm10 TimepointA_treatment1_treatment2_Diffpeaks_MotifOutput/ -size -300,100 -mask |
| Make BigWig Files | **makeBigWig.pl** sample-tagDir/ mm10 -strand + -webdir /path/to/html/ -url <url> |
| Nucleotide frequency histogram | **annotatePeaks.pl** <annotated peak file> mm10 -size 1000 -hist 1 -di <tagdirectory> |
| Annotate peaks for clustering | **annotatePeaks.pl** <peakfile> mm10 -fragLength 1 - strand + -d <tagdirectories> -rlog > outputfile.txt |

## 4.7 Supplementary Materials

### 4.7.1 Reagents

**Table 7: Reagent Recipes.** Volumes specified for one sample.

| Name | Components |
|---|---|
| TE'T | 0.05% Tween, 0.1 mM EDTA, 10 mM Tris pH 7.5 in $ddH_2O$ |
| TET | 0.05% Tween, 1 mM EDTA, 10 mM Tris pH 7.5 in $ddH_2O$ |
| Sequencing TET | 0.05% Tween, 0.1 mM EDTA, 10 mM Tris pH 8 in $ddH_2O$ |
| FLB | 5mM EDTA, 95% Formamide, bromophenol blue, xylene cyanol |
| Swelling Buffer | 10mM Tris-HCl pH 7.5, 2 mM $MgCl_2$, 3 mM $CaCl_2$, 2 U/mL Superase-IN in $ddH_2O$ |
| Lysis Buffer | Swelling Buffer + 1% IPEGAL |
| GRO Freezing Buffer | 40% Glycerol, 5 mM $MgCl_2$, 0.1 mM EDTA, 50 mM Tris-HCl (½ pH 8.0, ½ pH 7.5), 2 U/mL Superase-IN in $ddH_2O$ |
| START Elution Buffer | 400mM NaOAc, 0.05% Tween, 1 mM EDTA, 10 mM Tris pH 7.5 in $ddH_2O$ |
| SpeedBeads Mix | 3µL XP Beads, 41.5µL 5M NaCL, 41.5µL 40% PEG8000 |
| NEB Gel Elution Buffer | 0.5M LiCl, 0.1% SDS, 5mM EDTA, 10mM Tris pH 7.5 in $ddH_2O$ |
| DNA Extraction Buffer | 10mM Tris-HCl pH 8, 200mM NaCl, 0.5% SDS, 5mM EDTA |
| ATAC Elution Buffer | 10mM Tris-HCl pH 8.0 + 0.05% Tween |

### 4.7.2 GFP fluorescence in transfected RAW264.7 cells

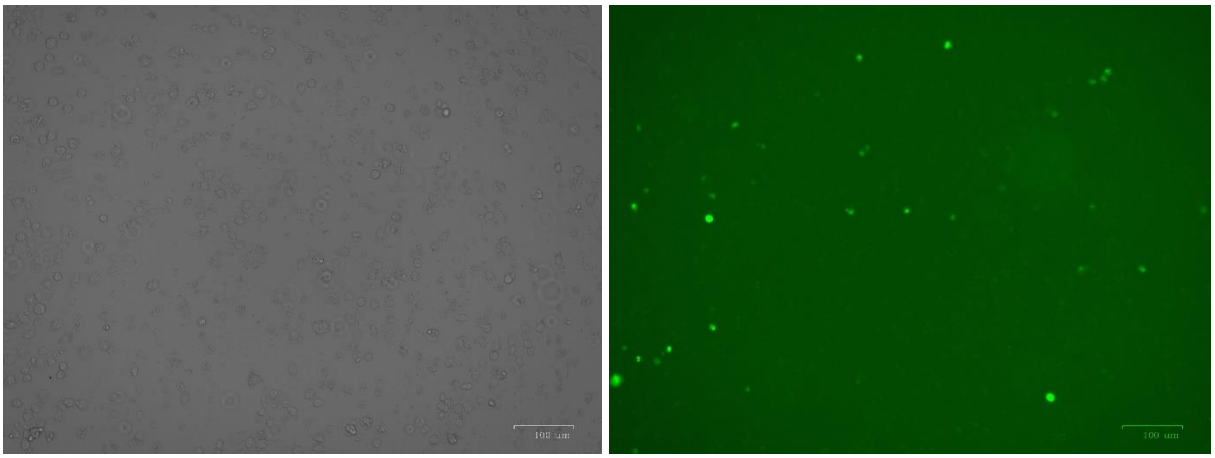

### 4.7.3 Table of Primers

**Table 8: List of Primers**. All primer sequences are written 5'-3'. Bolded sequences overlap the backbone reporter plasmid. Blue regions of primers for mutagenesis indicate overhangs.

| | |
|---|---|
| Oas3_nat_pro_F | **gccggtacctgagctcG**CAGATAATCTCAACAAACACCCTGAGCCT |
| Oas3_nat_pro_R | **ccaacagtaccggattgccA**TCTCCAGGGCTTCTTGGGGG |
| Tap1_nat_pro_F | **gccggtacctgagctcG**TGGGGAAGAAGAGGAGAATGAGATTCATG |
| Tap1_nat_pro_R | **ccaacagtaccggattgccA**GAAGGAGCAGGGCGGCC |
| Tgfbr1_nat_pro_F | **gccggtacctgagctcG**GAAACCCACGGCCGCTCAT |
| Tgfbr1_nat_pro_R | **ccaacagtaccggattgccA**GTCCCGCCGCCACTGT |
| MX2_nat_pro_F | **gccggtacctgagctcG**GGCAGGCACAGGCTGAATTAAGTT |
| MX2_nat_pro_R | **ccaacagtaccggattgccA**TCTTGACCTCAGCCCCAAGGG |
| MX2_nat_enh_F | **cctctacaaatgtggtaaaatcgataag**GGCAGGCACAGGCTGAATTAAGTT |
| MX2_nat_enh_R | **ggctctcaagggcatcgg**TCTTGACCTCAGCCCCAAGGG |
| Trim30c_nat_pro_F | **gccggtacctgagctcG**CAGTTCTCCACCTCCCCTTCCT |
| Trim30c_nat_pro_R | **ccaacagtaccggattgccA**CCAAGTTACTGGAAGGCAGAGCTG |
| Slfn9_nat_pro_F | **gccggtacctgagctcG**TGTAAGTTCTTGCTATAGGGAGGAAGCC |
| Slfn9_nat_pro_R | **ccaacagtaccggattgccA**AGAATTTAGAAACAGGCAGGAATGTAAGTCTCC |
| CD14_nat_pro_F | **gccggtacctgagctcG**TAATGATCTAAGGCACTAGGTGTGATTCACC |
| CD14_nat_pro_R | **ccaacagtaccggattgccA**AAGTTTGAGCAGCCCAGATAGGC |
| ADAR_nat_enh_F | **cctctacaaatgtggtaaaatcgataag**GTGTAAATGGTAGAGTACATGTAAGTTAAGC |

**Table 8: List of Primers Continued**. All primer sequences are written 5'-3'. Bolded sequences overlap the backbone reporter plasmid. Blue regions of primers for mutagenesis indicate overhangs.

| | |
|---|---|
| ADAR_nat_enh_R | **ggctctcaagggcatcgg**GTGTTTGAAGAGCCATGTTTGATATTATATGTTAGGATG |
| Ppp2r5c_nat_enh_F | **cctctacaaatgtggtaaaatcgataag**TATTCTAGCCATGAACTGGGTAAAAGTGTGC |
| Ppp2r5c_nat_enh_R | **ggctctcaagggcatcgg**CACTGAGAGGGTAGGCGGGAG |
| Synj1_nat_enh_F | **cctctacaaatgtggtaaaatcgataag**GTATGTCTGGACTGTTTGTGTCTCAGG |
| Synj1_nat_enh_R | **ggctctcaagggcatcgg**CTATAGAGTTGGCTTTTACAGCATTACATGAATTTAGA |
| Tbl2_nat_enh_F | **cctctacaaatgtggtaaaatcgataag**GAGGTAGTCTGATTGAATCCCTTCCTCAA |
| Tbl2_nat_enh_R | **ggctctcaagggcatcgg**TGGGCCAGCCTGCACTAAC |
| Tgfbr1_mut1_pro_F | CCAGGGCC**A**CGC**AA**GCGGGGCTCTCGGCTAGG |
| Tgfbr1_mut1_pro_R | GAGCCCCGC**TT**GCG**T**GGCCCTGGGCTACCAATGAG |
| Tgfbr1_mut2_pro_F | TAGGGCGCTCGC**AA**GCG**A**CGGGGGAGGCGGGGTC |
| Tgfbr1_mut2_pro_R | CCTCCCCCG**T**CGC**TT**GCGAGCGCCCTAGCGGGACCTA |
| CD14_mut_pro_F | CAATATTTACT**CCC**AGTGAGTAGGGCTGTTAGGAGGAAG |
| CD14_mut_pro_R | GCCCTACTCACT**GGG**AGTAAATATTGCAACGAAGTG |
| Tap1_mut_pro_F | CGAGGTCGGC**ATA**CGGTTTCTTCTTCCTCTAAAC |
| Tap1_mut_pro_R | GAAGAAACCG**TAT**GCCGACCTCGAATCACTAGAC |
| Trim30c_mut_pro_F | CCACAAGAG**CTC**TGAAAGTTAAGACTTTGAGGGGTG |
| Trim30c_mut_pro_R | CTTAACTTTC**AGA**GCTCTTGTGGTTCACCAGAGCC |
| Mx2_doublemut_pro_F | CAAGAACCAGAG**CTA**TG**ATA**GTGAAACTAAGTAGGAGCTGAG |
| Mx2_doublemut_pro_R | CTTAGTTTCAC**TAT**CA**TAG**CTCTGGTTCTTGGGGAACTTAATTCAG |
| Mx2_ISREmut_pro_F | GAAATGAAAGTG**ATA**CTAAGTAGGAGCTGAGCTGAGAAAG |
| Mx2_ISREmut_pro_R | CTCCTACTTAG**TAT**CACTTTCATTTCTCTGGTTCTTGGG |
| Mx2_T1mut_pro_F | CAAGAACCAGAG**CTA**TGAAAGTGAAACTAAGTAGGAGC |
| Mx2_T1mut_pro_R | CACTTTCA**TAG**CTCTGGTTCTTGGGGAACTTAATTCAG |
| Synth-PAmut_r | TCCTTATTTTCATTACATCTGTGTGT |
| pGL4seqLuc3'S | ATTTGTGATGCTATTGCTTTA |
| pGL4seqSalAS | CACCTGTCCTACGAGTTGCAT |

# 5 References

Andersson, R., Gebhard, C., Miguel-Escalada, I., Hoof, I., Bornholdt, J., Boyd, M., Chen, Y., Zhao, X., Schmidl, C., Suzuki, T., Ntini, E., Arner, E., Valen, E., Li, K., Schwarzfischer, L., Glatz, D., Raithel, J., Lilje, B., Rapin, N., Bagger, F., Jørgensen, M., Andersen, Peter Refsing, Bertin, N., Rackham, O., Burroughs, A. Maxwell Baillie, J. Kenneth Ishizu, Yuri, S., Yuri, F., Erina, Shiori, M., Yutaka, N., Christopher M., Meehan, T., Lassmann, T., Itoh, M., Kawaji, H., Kondo, N., Kawai, J., Lennartsson, A., Daub, C., Heutink, P., Hume, D., Jensen, T., Suzuki, H., Hayashizaki, Y., Müller, F., Forrest, A., Carninci, P., Rehli, M., Sandelin, A. (2014). An atlas of active enhancers across human cell types and tissues. *Nature*, *507*(7493), 455–461. https://doi.org/10.1038/nature12787

Antonelli, G., Scagnolari, C., Moschella, F., & Proietti, E. (2015). Twenty-five years of type I interferon-based treatment: A critical analysis of its therapeutic use. *Cytokine and Growth Factor Reviews*, *26*(2), 121–131. https://doi.org/10.1016/j.cytogfr.2014.12.006

Ayithan, N., Bradfute, S. B., Anthony, S. M., Stuthman, K. S., Bavari, S., Bray, M., & Ozato, K. (2015). Virus-Like Particles Activate Type I Interferon Pathways to Facilitate Post-Exposure Protection against Ebola Virus Infection. *PLOS ONE*, *10*(2), e0118345. https://doi.org/10.1371/journal.pone.0118345

Buenrostro, J. D., Giresi, P. G., Zaba, L. C., Chang, H. Y., & Greenleaf, W. J. (2013). Transposition of native chromatin for fast and sensitive epigenomic profiling of open chromatin, DNA-binding proteins and nucleosome position. *Nature Methods*, *10*(12), 1213–1218. https://doi.org/10.1038/nmeth.2688

Carlin, A. F., Plummer, E. M., Vizcarra, E. A., Sheets, N., Joo, Y., Tang, W., Day, J., Greenbaum, J., Glass, C. K., Diamond, M. S., & Shresta, S. (2017). An IRF-3-, IRF-5-, and IRF-7-Independent Pathway of Dengue Viral Resistance Utilizes IRF-1 to Stimulate Type I and II Interferon Responses. *Cell Reports*, *21*(6), 1600–1612. https://doi.org/10.1016/j.celrep.2017.10.054

Channappanavar, R., Fehr, A. R., Vijay, R., Mack, M., Zhao, J., Meyerholz, D. K., & Perlman, S. (2016). Dysregulated Type I Interferon and Inflammatory Monocyte-Macrophage Responses Cause Lethal Pneumonia in SARS-CoV-Infected Mice. *Cell Host and Microbe*, *19*(2), 181–193. https://doi.org/10.1016/j.chom.2016.01.007

Churchman, L. S., & Weissman, J. S. (2011). Nascent transcript sequencing visualizes transcription at nucleotide resolution. *Nature*, *469*(7330), 368–373. https://doi.org/10.1038/nature09652

Core, L. J., Waterfall, J. J., & Lis, J. T. (2008). Nascent RNA sequencing reveals widespread pausing and divergent initiation at human promoters. *Science*, *322*(5909), 1845–1848. https://doi.org/10.1126/science.1162228

Der, S. D., Zhou, A., Williams, B. R. G., & Silverman, R. H. (1998). Identification of genes

differentially regulated by interferon α, β, or γ using oligonucleotide arrays. *Proceedings of the National Academy of Sciences of the United States of America*, *95*(26), 15623–15628. https://doi.org/10.1073/pnas.95.26.15623

Diebold, S. S., Montoya, M., Unger, H., Alexopoulou, L., Roy, P., Haswell, L. E., Al-Shamkhani, A., Flavell, R., Borrow, P., & Reis e Sousa, C. (2003). Viral infection switches non-plasmacytoid dendritic cells into high interferon producers. *Nature*, *424*(6946), 324–328. https://doi.org/10.1038/nature01783

Donnelly, R. P., & Kotenko, S. V. (2010). Interferon-lambda: A new addition to an old family. In *Journal of Interferon and Cytokine Research* (Vol. 30, Issue 8, pp. 555–564). Mary Ann Liebert, Inc. 140 Huguenot Street, 3rd Floor New Rochelle, NY 10801 USA . https://doi.org/10.1089/jir.2010.0078

Dufour, C., Claudel, A., Joubarne, N., Merindol, N., Maisonnet, T., Masroori, N., Plourde, M. B., & Berthoux, L. (2018). Editing of the human TRIM5 gene to introduce mutations with the potential to inhibit HIV-1. *PLOS ONE*, *13*(1), e0191709. https://doi.org/10.1371/journal.pone.0191709

Duttke, S. H., Chang, M. W., Heinz, S., & Benner, C. (2019). Identification and dynamic quantification of regulatory elements using total RNA. *Genome Research*, *29*(11), 1836–1846. https://doi.org/10.1101/gr.253492.119

Franks, T. J., Chong, P. Y., Chui, P., Galvin, J. R., Lourens, R. M., Reid, A. H., Selbs, E., McEvoy, P. L., Hayden, D. L., Fukuoka, J., Taubenberger, J. K., & Travis, W. D. (2003). Lung pathology of severe acute respiratory syndrome (SARS): A study of 8 autopsy cases from Singapore. *Human Pathology*, *34*(8), 743–748. https://doi.org/10.1016/S0046-8177(03)00367-8

Gao, B., Wang, Y., Xu, W., Duan, Z., & Xiong, S. (2010). A 5′ Extended IFN-Stimulating Response Element Is Crucial for IFN-γ–Induced Tripartite Motif 22 Expression via Interaction with IFN Regulatory Factor-1. *The Journal of Immunology*, *185*(4), 2314–2323. https://doi.org/10.4049/jimmunol.1001053

Hemann, E. A., Gale, M., & Savan, R. (2017). Interferon lambda genetics and biology in regulation of viral control. *Frontiers in Immunology*, *8*(DEC), 1707. https://doi.org/10.3389/fimmu.2017.01707

Hervas-Stubbs, S., Perez-Gracia, J. L., Rouzaut, A., Sanmamed, M. F., Le Bon, A., & Melero, I. (2011). Direct effects of type I interferons on cells of the immune system. In *Clinical Cancer Research* (Vol. 17, Issue 9, pp. 2619–2627). American Association for Cancer Research. https://doi.org/10.1158/1078-0432.CCR-10-1114

Hu, X., & Ivashkiv, L. B. (2009). Cross-regulation of Signaling Pathways by Interferon-γ: Implications for Immune Responses and Autoimmune Diseases. In *Immunity* (Vol. 31, Issue 4, pp. 539–550). Cell Press. https://doi.org/10.1016/j.immuni.2009.09.002

Jafarzadeh, A., Nemati, M., Saha, B., Bansode, Y. D., & Jafarzadeh, S. (2020). Protective Potentials of Type III Interferons in COVID-19 Patients: Lessons from Differential Properties of Type I- and III Interferons. *Viral Immunology*, vim.2020.0076. https://doi.org/10.1089/vim.2020.0076

Jewell, N. A., Cline, T., Mertz, S. E., Smirnov, S. V., Flaño, E., Schindler, C., Grieves, J. L., Durbin, R. K., Kotenko, S. V., & Durbin, J. E. (2010). Lambda Interferon Is the Predominant Interferon Induced by Influenza A Virus Infection In Vivo. *Journal of Virology*, *84*(21), 11515–11522. https://doi.org/10.1128/jvi.01703-09

Juven-Gershon, T., Hsu, J. Y., Theisen, J. W., & Kadonaga, J. T. (2008). The RNA polymerase II core promoter - the gateway to transcription. In *Current Opinion in Cell Biology* (Vol. 20, Issue 3, pp. 253–259). NIH Public Access. https://doi.org/10.1016/j.ceb.2008.03.003

Kane, M., Yadav, S. S., Bitzegeio, J., Kutluay, S. B., Zang, T., Wilson, S. J., Schoggins, J. W., Rice, C. M., Yamashita, M., Hatziioannou, T., & Bieniasz, P. D. (2013). MX2 is an interferon-induced inhibitor of HIV-1 infection. *Nature*, *502*(7472), 563–566. https://doi.org/10.1038/nature12653

Killip, M. J., Fodor, E., & Randall, R. E. (2015). Influenza virus activation of the interferon system. *Virus Research*, *209*, 11–22. https://doi.org/10.1016/j.virusres.2015.02.003

Kindler, E., Thiel, V., & Weber, F. (2016). Interaction of SARS and MERS Coronaviruses with the Antiviral Interferon Response. In *Advances in Virus Research* (Vol. 96, pp. 219–243). Academic Press Inc. https://doi.org/10.1016/bs.aivir.2016.08.006

Kotenko, S. V., Gallagher, G., Baurin, V. V., Lewis-Antes, A., Shen, M., Shah, N. K., Langer, J. A., Sheikh, F., Dickensheets, H., & Donnelly, R. P. (2003). IFN-λs mediate antiviral protection through a distinct class II cytokine receptor complex. In *Nature Immunology* (Vol. 4, Issue 1, pp. 69–77). Nat Immunol. https://doi.org/10.1038/ni875

Kwak, H., Fuda, N. J., Core, L. J., & Lis, J. T. (2013). Precise maps of RNA polymerase reveal how promoters direct initiation and pausing. *Science*, *339*(6122), 950–953. https://doi.org/10.1126/science.1229386

Lam, M. T. Y., Cho, H., Lesch, H. P., Gosselin, D., Heinz, S., Tanaka-Oishi, Y., Benner, C., Kaikkonen, M. U., Kim, A. S., Kosaka, M., Lee, C. Y., Watt, A., Grossman, T. R., Rosenfeld, M. G., Evans, R. M., & Glass, C. K. (2013). Rev-Erbs repress macrophage gene expression by inhibiting enhancer-directed transcription. *Nature*, *498*(7455), 511–515. https://doi.org/10.1038/nature12209

Le Bon, A., Schiavoni, G., D'Agostino, G., Gresser, I., Belardelli, F., & Tough, D. F. (2001). Type I interferons potently enhance humoral immunity and can promote isotype switching by stimulating dendritic cells in vivo. *Immunity*, *14*(4), 461–470. https://doi.org/10.1016/S1074-7613(01)00126-1

Lei, X., Dong, X., Ma, R., Wang, W., Xiao, X., Tian, Z., Wang, C., Wang, Y., Li, L., Ren, L., Guo, F., Zhao, Z., Zhou, Z., Xiang, Z., & Wang, J. (2020). Activation and evasion of type I interferon responses by SARS-CoV-2. *Nature Communications*, *11*(1), 3810. https://doi.org/10.1038/s41467-020-17665-9

Lindenmann, J., Burke, D. C., & Isaacs, A. (n.d.). *STUDIES ON THE PRODUCTION, MODE OF ACTION AND PROPERTIES OF INTERFERON*.

McLaren, J. E., & Ramji, D. P. (2009). Interferon gamma: A master regulator of atherosclerosis. In *Cytokine and Growth Factor Reviews* (Vol. 20, Issue 2, pp. 125–135). Pergamon. https://doi.org/10.1016/j.cytogfr.2008.11.003

Murray, H. W. (1994). Interferon-gamma and host antimicrobial defense: Current and future clinical applications. In *The American Journal of Medicine* (Vol. 97, Issue 5, pp. 459–467). Elsevier. https://doi.org/10.1016/0002-9343(94)90326-3

Niewold, T. B. (2014). Type I Interferon in Human Autoimmunity. *Frontiers in Immunology*, *5*(JUN), 306. https://doi.org/10.3389/fimmu.2014.00306

Ozato, K., Shin, D. M., Chang, T. H., & Morse, H. C. (2008). TRIM family proteins and their emerging roles in innate immunity. In *Nature Reviews Immunology* (Vol. 8, Issue 11, pp. 849–860). Nature Publishing Group. https://doi.org/10.1038/nri2413

Pollard, K. M., Cauvi, D. M., Toomey, C. B., Morris, K. V., & Kono, D. H. (2013). Interferon-gamma and systemic autoimmunity. *Discovery Medicine*, *16*(87), 123–131. /pmc/articles/PMC3934799/?report=abstract

Pott, J., Mahlakõiv, T., Mordstein, M., Duerr, C. U., Michiels, T., Stockinger, S., Staeheli, P., & Hornef, M. W. (2011). IFN-λ determines the intestinal epithelial antiviral host defense. *Proceedings of the National Academy of Sciences of the United States of America*, *108*(19), 7944–7949. https://doi.org/10.1073/pnas.1100552108

Psarras, A., Emery, P., & Vital, E. M. (2017). Type I interferon-mediated autoimmune diseases: Pathogenesis, diagnosis and targeted therapy. In *Rheumatology (United Kingdom)* (Vol. 56, Issue 10, pp. 1662–1675). Oxford University Press. https://doi.org/10.1093/rheumatology/kew431

Pulit-Penaloza, J. A., Scherbik, S. V., & Brinton, M. A. (2012). Activation of Oas1a gene expression by type I IFN requires both STAT1 and STAT2 while only STAT2 is required for Oas1b activation. *Virology*, *425*(2), 71–81. https://doi.org/10.1016/j.virol.2011.11.025

Rawlings, J. S., Rosler, K. M., & Harrison, D. A. (2004). The JAK/STAT signaling pathway. *Journal of Cell Science*, *117*(8), 1281–1283. https://doi.org/10.1242/jcs.00963

Read, S. A., Wijaya, R., Ramezani-Moghadam, M., Tay, E., Schibeci, S., Liddle, C., Lam, V. W.

T., Yuen, L., Douglas, M. W., Booth, D., George, J., & Ahlenstiel, G. (2019). Macrophage Coordination of the Interferon Lambda Immune Response. *Frontiers in Immunology*, *10*. https://doi.org/10.3389/fimmu.2019.02674

Sadler, A. J., & Williams, B. R. G. (2008). Interferon-inducible antiviral effectors. In *Nature Reviews Immunology* (Vol. 8, Issue 7, pp. 559–568). Nature Publishing Group. https://doi.org/10.1038/nri2314

Schwalb, B., Michel, M., Zacher, B., Hauf, K. F., Demel, C., Tresch, A., Gagneur, J., & Cramer, P. (2016). TT-seq maps the human transient transcriptome. *Science*, *352*(6290), 1225–1228. https://doi.org/10.1126/science.aad9841

Secombes, C. J., & Zou, J. (2017). Evolution of interferons and interferon receptors. In *Frontiers in Immunology* (Vol. 8, Issue MAR, p. 209). Frontiers Research Foundation. https://doi.org/10.3389/fimmu.2017.00209

Sheppard, P., Kindsvogel, W., Xu, W., Henderson, K., Schlutsmeyer, S., Whitmore, T. E., Kuestner, R., Garrigues, U., Birks, C., Roraback, J., Ostrander, C., Dong, D., Shin, J., Presnell, S., Fox, B., Haldeman, B., Cooper, E., Taft, D., Gilbert, T., Grant, Francis J., Tackett, M., Krivan, W., McKnight, G., Clegg, C., Foster, D., Klucher, K. M. (2003). IL-28, IL-29 and their class II cytokine receptor IL-28R. In *Nature Immunology* (Vol. 4, Issue 1, pp. 63–68). Nature Publishing Group. https://doi.org/10.1038/ni873

Stark, G. R., Kerr, I. M., Williams, B. R. G., Silverman, R. H., & Schreiber, R. D. (1998). How cells respond to interferons. In *Annual Review of Biochemistry* (Vol. 67, pp. 227–264). Annual Reviews 4139 El Camino Way, P.O. Box 10139, Palo Alto, CA 94303-0139, USA . https://doi.org/10.1146/annurev.biochem.67.1.227

Steimle, V., Siegrist, C. A., Mottet, A., Lisowska-Grospierre, B., & Mach, B. (1994). Regulation of MHC class II expression by interferon-γ mediated by the transactivator gene CIITA. *Science*, *265*(5168), 106–109. https://doi.org/10.1126/science.8016643

Takeuchi, O., & Akira, S. (2010). Pattern Recognition Receptors and Inflammation. In *Cell* (Vol. 140, Issue 6, pp. 805–820). Cell Press. https://doi.org/10.1016/j.cell.2010.01.022

Thimme, R., Oldach, D., Chang, K. M., Steiger, C., Ray, S. C., & Chisari, F. V. (2001). Determinants of viral clearance and persistence during acute hepatitis C virus infection. *Journal of Experimental Medicine*, *194*(10), 1395–1406. https://doi.org/10.1084/jem.194.10.1395

Tumpey, T. M., Szretter, K. J., Van Hoeven, N., Katz, J. M., Kochs, G., Haller, O., García-Sastre, A., & Staeheli, P. (2007). The Mx1 Gene Protects Mice against the Pandemic 1918 and Highly Lethal Human H5N1 Influenza Viruses. *Journal of Virology*, *81*(19), 10818–10821. https://doi.org/10.1128/jvi.01116-07

*Virus interference. I. The interferon* (Vol. 8). (n.d.).

Wissink, E. M., Vihervaara, A., Tippens, N. D., & Lis, J. T. (2019). Nascent RNA analyses: tracking transcription and its regulation. In *Nature Reviews Genetics* (Vol. 20, Issue 12, pp. 705–723). Nature Publishing Group. https://doi.org/10.1038/s41576-019-0159-6

Wittkopp, P. J., & Kalay, G. (2012). Cis-regulatory elements: Molecular mechanisms and evolutionary processes underlying divergence. In *Nature Reviews Genetics* (Vol. 13, Issue 1, pp. 59–69). Nature Publishing Group. https://doi.org/10.1038/nrg3095

Wong, M. T., & Chen, S. S. L. (2016). Emerging roles of interferon-stimulated genes in the innate immune response to hepatitis C virus infection. In *Cellular and Molecular Immunology* (Vol. 13, Issue 1, pp. 11–35). Chinese Soc Immunology. https://doi.org/10.1038/cmi.2014.127

Wynn, T. A., Chawla, A., & Pollard, J. W. (2013). Macrophage biology in development, homeostasis and disease. In *Nature* (Vol. 496, Issue 7446, pp. 445–455). Nature Publishing Group. https://doi.org/10.1038/nature12034

Xia, H., Cao, Z., Xie, X., Zhang, X., Chen, J. Y. C., Wang, H., Menachery, V. D., Rajsbaum, R., & Shi, P. Y. (2020). Evasion of Type I Interferon by SARS-CoV-2. *Cell Reports*, *33*(1), 108234. https://doi.org/10.1016/j.celrep.2020.108234

Zhou, Y., Zhou, B., Pache, L., Chang, M., Khodabakhshi, A. H., Tanaseichuk, O., Benner, C., & Chanda, S. K. (2019). Metascape provides a biologist-oriented resource for the analysis of systems-level datasets. *Nature Communications*, *10*(1). https://doi.org/10.1038/s41467-019-09234-6